


Peer review status:

This is a non-peer-reviewed preprint submitted to EarthArXiv.
This manuscript is under review at Journal of Climate.

File generated with AMS Word template 2.0

# Attribution of climate extremes with global temperature regressions: accounting for uncertainty from internal variability

Maximilian Kotz,[a, b, c] Markus G. Donat,[a, d]

[a] *Barcelona Supercomputing Center, Barcelona, Spain*

[b] *Potsdam Institute for Climate Impact Research, Potsdam, Germany*

[c] *Centre for Biodiversity and Conservation Science, University of Queensland, Brisbane, Australia*

[d] *Institució Catalana de Recerca i Estudis Avançats (ICREA), Barcelona, Spain*

*Corresponding author*: Maximilian Kotz, maximilian.kotz@bsc.es



File generated with AMS Word template 2.0

## ABSTRACT

Attribution of climate change to anthropogenic forcing is an important goal in climate science. Regression of local conditions on global temperatures is a popular statistical approach, but whether the uncertainty derived from observations alone can reflect the range of outcomes possible due to internal variability remains unclear. Here, we use large ensembles from three climate models as an idealized testbed to quantify the role of internal variability for such attribution of climate extremes with single climate realisations. Internal variability generates large uncertainty in the linear-regression slope between global temperatures and regional temperature extremes, exceeding 40% of the ensemble mean slope across 50, 38, and 9% of the global surface area in the MIROC6, MPI-ESM1-2-LR and CanESM5 models respectively. Nevertheless, we show that these uncertainties can be accurately inferred from individual ensemble members using a block-bootstrap procedure - offering potential for a robust application to observations. Block-bootstrapping also accurately captures the absolute uncertainty for precipitation extremes, despite a substantially smaller signal-to-noise ratio which leads to underestimated and overly noisy estimates of relative uncertainty at present-day warming levels. This work provides a basis for the attribution of climate extremes from observations which can robustly capture the uncertainty associated with internal climate variability.


## SIGNIFICANCE STATEMENT

Attribution of climate changes is crucial to many aspects of climate policy regarding adaptation, mitigation and climate justice. Approaches using regressions of observed regional climate conditions on global temperatures are increasingly popular, especially for the attribution of downstream impacts e.g. on human health. Confidence in these methods relies on correlations having been unlikely to occur due to internal variability alone. We test these approaches with large ensembles, finding large uncertainties due to internal variability. We show that for attribution of temperature and precipitation extremes, robust confidence intervals can be recovered from individual ensemble members via block-bootstrapping. This provides a robust basis for attribution of climate extremes and impacts with observations alone.



File generated with AMS Word template 2.0

## 1. Introduction

As global temperatures continue to rise and are set to pass internationally agreed limits of 1.5C within the coming decades (Bevacqua et al. 2025), understanding the impacts of climate change gains further relevance (Allen et al. 2019). The increasing exposure to high temperature and heavy precipitation extremes is of particular concern given their known impact on socioeconomic (Kotz et al. 2022; Callahan and Mankin 2022; Davenport et al. 2021) and natural systems (Kotz et al. 2025; Murali et al. 2023). At the regional level, increases in these extremes scale with global mean surface temperature (GMST) and therefore with increasing cumulative human emissions (Seneviratne et al. 2016). Formalising the attribution of these extremes and their impacts to human influence remains an important and active area of climate science with ongoing challenges and developments (Trok et al. 2024; Clarke et al. 2022), especially for attribution of impacts (King et al. 2023; Noy et al. 2023).

Early IPCC guidelines on attribution laid out separate stages for the detection of changes in observations using statistical methods, and the attribution of those changes to human influence based on counterfactual simulations of General Circulation and Earth System Models (GCMs/ESMs) in the absence of anthropogenic emissions (Hegerl et al. 2007; Gillett et al. 2016). Often conducted with an optimal-fingerprinting analysis (Hegerl et al. 1996), a central goal of these approaches is to distinguish between changes which could have occurred due to internal variability alone and those which could not. However, as the strength of the anthropogenic signal has become the increasingly dominant source of multidecadal change (Arias et al. 2021) - particularly for temperature - statistical methods which aim to identify the forced signal of climate change directly from observations have proliferated and gained traction (Wills et al. 2026), gaining particular popularity for attributing downstream sectoral impacts (Mengel et al. 2021). Key benefits of these approaches are their low computational requirements and the avoidance of certain trend biases which climate models are known to exhibit (Wills et al. 2022; Donat et al. 2023).

Amongst these statistical methods, the linear regression of regional climate conditions on GMST is a popular approach. Two major examples of its use are for Extreme Event



File generated with AMS Word template 2.0

Attribution using Generalised Extreme Value functions (Van Oldenborgh et al. 2021), and for de-trending methodologies used to generate counterfactuals for impact-attribution (Mengel et al. 2021). These methods are motivated by the fact that virtually all of the observed historical global warming signal (0.84-1.10C between 1850-1900 and 2001-2020) is attributable to human influence (likely range of human contribution of 0.8-1.3C) (Lee et al. 2023) and that forced changes in extremes are known to scale linearly with GMST in scenarios with monotonically increasing forcing (Seneviratne et al. 2016), although hysteresis has been reported in overshoot scenarios (Roldán-Gómez et al. 2025; Pfleiderer et al. 2024). The particular uptake of GMST regressions for counterfactual generation and the attribution of downstream impacts on marine heatwaves (Marcos et al. 2025), streamflow changes (Wang et al. 2025), health (Beck et al. 2024; Dimitrova et al. 2024; Erazo et al. 2024) and biodiversity (Kotz et al. 2025) underscores the widespread potential of this method and the importance of understanding its robustness.

Despite the promise of widespread application, it remains unclear whether uncertainty estimates from GMST-regression approaches to attribution and counterfactual generation reflect the full range of outcomes possible due to internal variability. For example, widely-used sources of counterfactual climate data for impact attribution based on this approach do not yet provide quantification of uncertainty at all (Mengel et al. 2021; Dimitrova et al. 2024). Studies which do provide uncertainty estimates typically report parametric uncertainty from the GMST-regression (Beck et al. 2024; Van Oldenborgh et al. 2021), but whether this reflects the actual range of outcomes which could be possible under different realisations of climate variability is so far unquantified. Given the substantial contributions of internal variability to regional climate trends (Hawkins and Sutton 2009; Lehner et al. 2020), especially under historical levels of anthropogenic forcing and for variables such as precipitation (Deser et al. 2012), this represents a major limitation in the development of robust impact-attribution statements. Community initiatives have tested how well a statistically detected trend matches the average of a large ensemble, including when using GMST-regression (Wills et al. 2025), but the extent to which uncertainty in the statistically detected changes reflects the full range of possible outcomes under different realisations of internal climate variability has not yet been tested. This has particular relevance for downstream applications to attribution with observations wherein uncertainty



File generated with AMS Word template 2.0

in the human-driven component of change determines the strength of the attribution statement.

Our paper aims to quantify the role of internal variability in GMST-regression based attribution methods, using large ensembles of climate models as an idealised setting to test these approaches. Large ensembles involve simulations of a given climate model under the same climate forcing, with variations in initial conditions used to generate diverse realisations of internal climate variability within which the ensemble mean represents the expected response to forcing. Our paper has three main objectives: (1) to quantify the uncertainty in the relationships between GMST and regional climate conditions driven by internal variability; (2) to test whether statistical methods could theoretically infer these uncertainties when applied to individual realisations of the climate system; and (3) to apply such methods to observational data. We focus our analysis on the frequency and intensity of climate extremes, given their important role for impacts as reflected in recent work on the economy (Callahan and Mankin 2022) and biodiversity (Kotz et al. 2025). We consider both temperature and precipitation extremes, to explore variables for which the relative importance of internal variability and anthropogenic forcing differs.

## 2. Methods

### *Data*

We use data of daily average surface temperature ("tas") and daily precipitation sums ("pr") from three Earth System Models providing large ensembles within the Coupled Model Intercomparison Project phase 6 (Eyring et al. 2016) (CanESM5, MIROC6 and MPI-ESM1-2-LR), each with 50 ensemble members based on different initialisations. We primarily use data from simulations under the historical forcing scenario, using data from 1940 onwards to replicate the time-frame of availability in the ERA-5 reanalysis (Hersbach et al. 2020). We additionally use data from simulations for the period 2015-2024 under the SSP5-8.5 forcing scenario, to provide a full time-series until 2024 which more closely matches the data period available from ERA-5. We note that the radiative forcing is similar across other scenarios between 2014 and 2024 (Riahi et al. 2017) and would therefore likely provide similar results. Moreover, we emphasise that we only use these simulations to test attribution methodologies in an idealised setting rather than to make predictions about



File generated with AMS Word template 2.0

developments over the period 2015-2024. We also use data on daily surface temperature and precipitation from the ERA-5 reanalysis for the period 1940-2024 (Hersbach et al. 2020).

### *Climate extreme metrics*

We use two complementary metrics to capture the intensity and frequency of climate extremes. We use the annual maximum of 5 day averages of daily average temperature and daily total precipitation (here referred to as $T5dx$, $P5dx$) to measure the intensity of multi-day climate extremes which are relevant for impacts (Callahan and Mankin 2022). We also use the annual number of days exceeding the 99th percentile of the historical distribution ($T99p$, $P99p$) - using the period 1940-1970 and a consideration of all seasons to define these thresholds. This choice focuses on the exceedance of absolute temperature and precipitation thresholds rather than seasonally-defined thresholds, as has been shown to be relevant for impacts (Kotz et al. 2025). We use the threshold obtained from the historical period of each ensemble member separately (rather than taking an average across ensemble members), such that each ensemble member is treated independently as would be the case when applying such attribution methods to observations which we aim to test.

### *Global-temperature based attribution*

The climate impact attribution literature typically uses smoothed GMST to fit a linear relationship between large-scale forcing and local climate conditions, with which to then detrend local climate conditions and generate a counterfactual (Mengel et al. 2021). We calculate GMST as the area weighted average of daily surface temperature ($GMT_{m,y}$) for each ensemble member, *m*, and year, *y*, and smooth it with an 11-year running mean centered on the year of interest. We then fit linear relationships between smoothed GMST ($\widetilde{GMT}_{m,y}$) and local climatic conditions ($T5dx_{m,x,y}$, $P5dx_{m,x,y}$, $T99p_{m,x,y}$, $P99p_{m,x,y}$) at each grid-cell, *x*, for each ensemble member, m, using linear Ordinary Least Squares regression for the climate extreme intensity metrics:

$$T5dx_{m,x,y} = \beta_{m,x}\,\widetilde{GMT}_{m,y} + \alpha_{m,x} + \epsilon_{m,x,y} \quad (1)$$



File generated with AMS Word template 2.0

where $\beta_{m,x}$ is the linear relationship between global temperatures and local climate extremes for each ensemble member and grid cell, $x$, $\alpha_{m,x}$ is the intercept, and $\epsilon_{m,x,y}$ the error term. We note that the local climate conditions themselves are not smoothed.

For metrics of climate extreme frequency, we instead use a linear Poisson model - designed specifically for count data:

$$log(E(T99p_{m,x,y} \mid \widetilde{GMT}_{m,y})) = \beta_{m,x}\widetilde{GMT}_{m,y} + \alpha_{m,x} + \epsilon_{m,x,y}, \quad (2)$$

in which case the coefficient $\beta_{m,x}$ denotes the expected change in the logarithm of the number of days exceeding the climate extreme threshold for each change in the GMST.

In both the linear and Poisson model cases outlined in equations 1 and 2, the attributable climate change signal essentially depends on the estimates of $\beta_{m,x}$, which represents the scaling relationship between GMST and local extremes, and on which we therefore focus our assessment of uncertainty due to internal climate variability.

*Uncertainty due to internal variability*

We evaluate uncertainty in climate impact attribution approaches due to internal variability based on the spread of estimates of $\beta_{m,x}$ across ensemble members. We express this through both the absolute uncertainty - the standard deviation of estimates across ensemble members. $\sigma_x(\beta_{m,x})$ - as well as the relative uncertainty, measured as the ratio of the standard deviation, to the mean, $\mu_x(\beta_{m,x})$, of these estimates across ensemble members:

$$\chi_x = 100 * \frac{\sigma_x(\beta_{m,x})}{\mu_x(\beta_{m,x})}. \quad (3)$$

We proceed with these calculations separately for each climate extreme metric and each of the three large ensembles.

*Block-bootstrap estimates of uncertainty*



File generated with AMS Word template 2.0

The multiple realisations of the simulated climate system within the large ensembles provide an idealised setting in which to evaluate the uncertainty due to internal variability inherent in these climate impact-attribution approaches. However, approaches based on observations will always be constrained to work with a single realisation of the climate system. We therefore propose block-bootstrapping as a potential method to infer estimates of uncertainty from individual realisations which might reflect the uncertainty driven by internal variability. Similar approaches have been used to construct so-called "observational large ensembles" (McKinnon et al. 2017; McKinnon and Deser 2018) and we draw on the intuition of these approaches in the context of attribution.

Block-bootstrapping generates synthetic time series by sampling contiguous blocks of the original time series (with replacement) to create a new artificial time series of the original data. This can provide an accurate reflection of uncertainty in certain statistical properties of the data if the synthetic time-series retains the auto-correlation structure of the original data within the blocks (McKinnon et al. 2017; McKinnon and Deser 2018). Our block-bootstrap approach only samples across time, thereby preserving all spatial autocorrelation structure. The most important choice in our block-bootstrap approach is therefore the choice of block width which determines how much of the temporal autocorrelation structure of the original data is preserved. The block width should be sufficiently large to capture the autocorrelation structure of the internal variability which contributes to uncertainty in the forced trend, but should be small enough to enable a large number of block samples. A block width which is too small may underestimate uncertainty by ignoring processes which are important sources of temporal autocorrelation, whereas a block width which is too large may overestimate uncertainty by causing insufficient blocks to be available to generate a sufficient number of bootstrap samples. For example, block widths of one year produce time series with 85 randomly selected blocks (for the 85-year 1940-2024 time period), whereas block widths of 5 years produce time series derived from 17 randomly-selected, contiguous blocks. We consistently sample from both local climate conditions and GMST to preserve their correlation structure which reflects the attribution relationship we aim to identify.

To inform our choice of the block width, we therefore calculate the autocorrelation function of the residuals of the regressions between global temperatures and local climate conditions (Figures A2-A4), using the actual residuals in the case of the extreme intensity metrics and



File generated with AMS Word template 2.0

the residuals on the deviance scale for the Poisson regressions applied to the frequency metrics - both of these are represented as $\epsilon_{m,x,y}$ in equations (1) and (2). We use plots of the autocorrelation strength to guide the choice of block widths, and explore results under a range of block widths as outlined in the results section. Variance estimates of the autocorrelation functions are calculated using Bartlett's formula (Bartlett 1946) and two sided significance tests are calculated for each ensemble member. The residuals of temperature extremes show significant autocorrelation up to 3 years in the tropics, decaying more quickly over land regions and within CanESM5 (Figures A2-4). Residuals of precipitation extremes show similar patterns. We therefore use a primary block width of 5 years such that individual blocks retain relevant information on internal variability, while testing our results for smaller and larger block sizes.

We apply consistent block sampling across different grid-cells and different members of the same large ensemble, and then re-evaluate the regressions outlined in equations (1) and (2). We use 100 samples with replacement ($N_s = 100$). Note that, unlike McKinnon et al. (2017), who block-bootstrap residuals around an estimated forced component, we resample blocks of paired (GMST, local extreme) values and re-estimate the regressions, i.e. a block 'pairs' bootstrap. This choice is motivated by (i) our investigation of a Poisson regression for frequency metrics, for which residual resampling is ill-suited, as resampling residuals on the deviance scale could result in non-integer and even negative counts for the $T99p$, $P99p$ metrics; (ii) potential heteroskedasticity due to changes in the variance of extremes with warming which would not be preserved by a residual bootstrap, most relevant given increasing precipitation variability with global warming (Zhang et al. 2021); and (iii) our aim of estimating the sampling distribution of the regression coefficient - for which a paired bootstrap is the textbook approach - rather than generating synthetic time series.

These samples provide us with a distribution of the relationship between global temperature and local climate extremes for each individual ensemble member, $\hat{\beta}_{s,m,x}$, with which we can estimate the absolute uncertainty, $\sigma_{m,x}(\beta_{s,m,x})$, and relative uncertainty in these relationships derived from the bootstrap:

$$\hat{\chi}_{m,x} = 100 * \frac{\sigma_{m,x}(\beta_{s,m,x})}{\mu_{m,x}(\beta_{s,m,x})}. \quad (4)$$



File generated with AMS Word template 2.0

Note that this estimate of relative uncertainty via bootstrapping is therefore available for each individual ensemble member. We then compare estimates of uncertainty derived from the bootstrap approach (equation 4) to those derived from the true ensemble (equation 3), to test the ability of the bootstrap to reproduce uncertainty due to internal variability as estimated from the large ensemble simulations. We do so based on a range of approaches (see next section, “Evaluation of the block-bootstrap estimates of uncertainty”).

The relative uncertainty is poorly defined in regions where $\mu_{m,x}$ approaches zero, and in some instances can therefore diverge strongly and bias the values of the weighted pattern correlation statistics. For the calculation of the weighted pattern correlation statistics, we therefore cap values of relative uncertainty at 100%. This choice is also motivated by the fact that values of relative uncertainty greater than 100% reflect instances of signal-to-noise ratio less than 1 in which a robust attribution to human influence is essentially not possible. Differences in values already greater than 100% are therefore not of substantial interest in the context of attribution.

Finally, we apply the block-bootstrap procedure outlined here to ERA-5 reanalysis data from 1940-2025 as a representation of real-world climate changes, carrying out the procedures described above with the distinction that in this case only one realisation of the (real-world) climate system is available. Having calculated the linear regression of local conditions on GMST using linear-regression (equation 1), we quantify a distribution of the linear-regression slopes ($\beta_x$) based on block-bootstrapping with a block-width of 5 years using the methods outlined above. We then detrend the observations based on this linear-regression by subtracting the product of $\beta_x$ and the smoothed GMST time-series from the observed conditions. We note that in the context of observations or reanalysis where only a single climate realisation is available, no assessment of the forced response in terms of the mean across realisations of internal variability can be made, but an assessment of uncertainty in the observed response due to internal variability is possible (McKinnon et al. 2017).

*Evaluation of the block-bootstrap estimates of uncertainty*



File generated with AMS Word template 2.0

We provide a range of metrics to evaluate the representation of uncertainty by the bootstrap of individual ensemble members with reference to the uncertainty estimated from the large ensemble. First, we evaluate the area-weighted fraction of the global surface area which is below a given level of relative uncertainty in both the bootstrapped individual ensemble members and large ensemble to compare the general level of uncertainty represented by each approach (see e.g. Figure 3a). Second, we calculate area-weighted, centred pattern correlation statistics between the uncertainty maps derived from both the bootstrapped individual ensemble members and the large ensemble. We do this for both the relative (as in Figure 3c) and absolute uncertainty (as in Figure 5b). To further assess whether the extent to which these pattern correlations reflect substantial differences between climate models, we assess these correlations between each individual ensemble member and the large ensemble to which it belongs, as well as to the other two large ensemble members based on a different climate model (as in Figure 3d). When making this comparison of pattern correlations between different climate model ensembles, we first re-grid all uncertainty maps to a common grid (that of the coarsest climate model, CanESM5) using a first-order conservative remapping (from xESMF). Finally, we calculate precision metrics for the uncertainty maps derived from block-bootstraps of individual ensemble members, comparing them to the uncertainty derived from the large ensemble as an estimate of the ground truth. Precision is here defined as the area-weighted fraction of grid-cells which are identified by the bootstrap as having uncertainty below a given level and in which the uncertainty as represented by the large ensemble is also below that level. By evaluating the fraction of predictions of low uncertainty which are accurately correct, this metric reflects the potential confidence of attribution statements made on the basis of this method. For comparison, we also compare this precision level to that which would be obtained with the expected precision of a random guess (with 50% likelihood of success) of whether a grid-cell is below a given level of uncertainty.

## 3. Results

*Internal variability generates diverse attribution outcomes for climate extremes*



File generated with AMS Word template 2.0

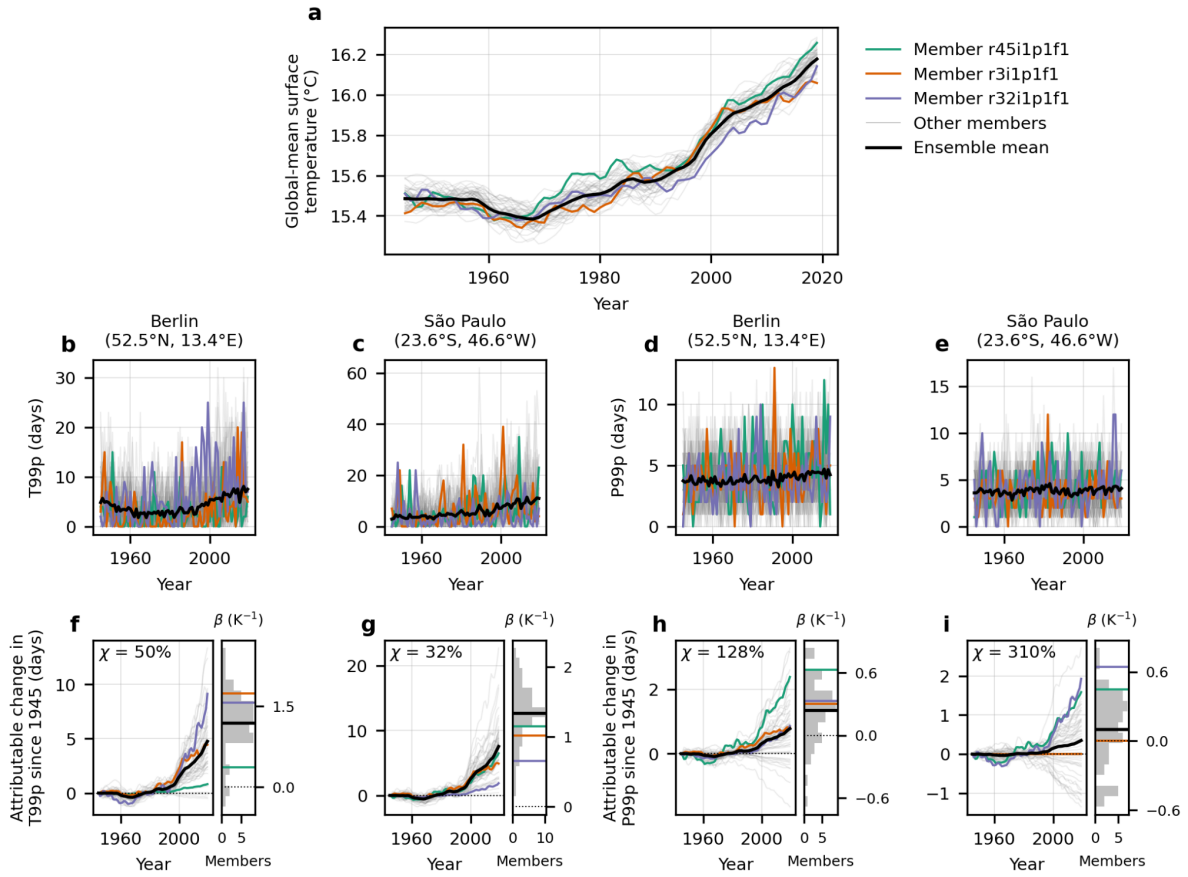



***Figure 1. Internal variability generates diverse relationships between global temperatures and local climate extremes.*** (a) Global temperatures smoothed with an 11-year centred running mean from 50 members of the MIROC6 ensemble under historical (1945-2014) and SSP5-8.5 (2015-2020) forcing are shown in light grey, with three ensemble members shown coloured for illustration purposes, and the ensemble mean in black. The annual number of days exceeding the 99th percentile of temperature (b, c) and precipitation (d, e) across the members of the MIROC6 ensemble under the same forcing, for grid-cells in Berlin and Sao Paolo (the coordinates in degrees latitude and longitude are indicated above each panel). Time-series of the attributable change in local temperature (f, g) and precipitation extremes (h, i), based on a linear Poisson regression with global mean surface temperature (see Methods) are shown. The distribution of regression slopes (β) with the global mean temperature are shown adjacent, with their relative uncertainty (χ) across ensemble members shown inset.

Comparing global temperatures and regional climate extremes across realisations of the same climate model under the same forcing, we see that local climate extremes can evolve in diverse ways despite similar evolutions of the GMST (Figure 1a-e). Moreover, the component of local climate extremes which is correlated with GMST also differs substantially across different realisations of the same model (Figure 1f-i). This highlights the diverse outcomes which could be attributed to human-induced climate change under observationally-derived attribution approaches using GMST-regression due to the uncertainty generated by internal variability. Figure 1 shows examples for the frequency of temperature



File generated with AMS Word template 2.0

and precipitation extremes ($T99p$, $P99p$), while Figure A1 shows similar behaviour for the intensity of extremes ($T5dx$, $P5dx$).

To formally quantify the role of internal variability, we calculate the absolute uncertainty (standard deviation) and relative uncertainty (standard deviation as a percentage of the mean) in the coefficients of the regressions between GMST and local climate extremes across different realisations of the same climate model. The relative uncertainty reflects the magnitude of uncertainty in the relationship with GMST as well as the uncertainty in this relationship, both crucial for quantifying anthropogenic contributions to local climate change. For temperature extremes, we see diversity across regions and climate models in the magnitude of relative uncertainty due to internal climate variability (Figure 2a, e, i). Uncertainty is largest in the Southern Ocean and South-East Pacific, where it exceeds 100% in many regions in all models. Such high levels of uncertainty are also found across further widespread areas in the MIROC6 and MPI-ESM1-2-LR climate models, particularly across central Africa, the Indian sub-continent and Tibetan plateau. In general, CanESM exhibits generally lower levels of relative uncertainty likely reflecting its larger climate sensitivity and therefore stronger signal-to-noise ratio of temperature extreme change (Swart et al. 2019).

We note that levels of uncertainty above 100% imply a signal to noise ratio between the forced climate change signal and internal variability of less than 1, which would typically preclude a robust statement regarding attribution of human-driven temperature extreme change. This demonstrates the importance of accounting for uncertainty due to internal climate variability in observationally-derived attribution approaches. Nevertheless, the large ensembles indicate that for temperature extremes 80%, 85% and 95% of the global area exhibits uncertainties less than 100% for MIROC6, MPI-ESM1-2-LR and CanESM5 respectively, and 50, 62, and 91% exhibit uncertainties under 40% (Figure 3a). Our analysis of these models therefore suggests that robust attribution with single realisations may be feasible for temperature extremes across large areas of the Earth. However, the diverse levels of uncertainty between climate models begs the question of what the true level of uncertainty in observations may be, and whether this could be inferred directly from observations.



File generated with AMS Word template 2.0

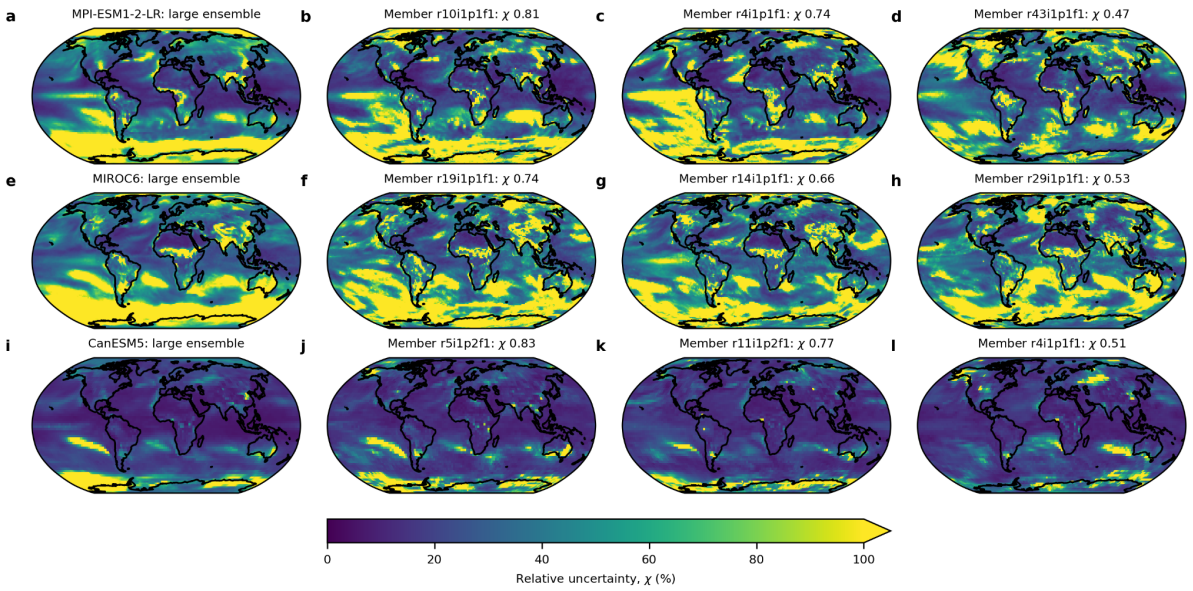



***Figure 2. Relative uncertainty in the attribution of heat extreme frequency due to internal variability in the large ensembles and as inferred from block-bootstrapping of individual ensemble members.*** The relative uncertainty (ratio of standard deviation to the mean, $\chi$) of the linear-regression slope between global temperatures and the frequency of temperature extremes, estimated from the large ensemble (a, e, i) and by block-bootstrapping individual ensemble members (b-d, f-h, j-l). Examples are shown for three ensemble members with the highest (b, f, j), median (c, g, k) and lowest (d, h l) area-weighted pattern correlation between their uncertainty and that derived from the large ensemble. These area-weighted pattern correlations are shown above the map for each ensemble member. Results are shown for the MPI-ESM1-2-LR (a-d), MIROC6 (e-h) and CanESM5 (i-l) models.

### *Reproducing uncertainty from individual realisations with a block-bootstrap*

We suggest that block-bootstrapping may offer the potential to infer the uncertainty due to internal climate variability from single realisations, which would imply potential for a robust application to observations. This hypothesis is partially motivated by "observational large ensembles" which have successfully used bootstrapping to develop ensembles of temperature trends from observations which accurately reflect the uncertainty due to internal variability (McKinnon et al. 2017). Block-bootstrapping individual ensemble members and re-calculating the relative uncertainty across bootstrap samples produces patterns of uncertainty which match those derived from the large ensemble for temperature extremes (Figure 2b-d, f-h, j-l). While the performance of the bootstrap can vary across ensemble members and shows differences in certain regions (Figure 2b-d, f-h, j-l), we note that it is clearly able to capture the spatial patterns within each model and broad differences between climate models (comparing different rows of Figure 2).



File generated with AMS Word template 2.0

Specifically, block-bootstrapping skilfully reproduces the fractions of the global surface-area under different levels of uncertainty (Figure 3a). The precision of the block-bootstrap in correctly identifying areas with relative uncertainty below a certain threshold is also high - exceeding 0.85 across climate models for a level of uncertainty of 60% - and substantially higher than the expectation from a random guess (Figure 3b). Furthermore, area-weighted pattern correlations between the uncertainty maps derived from the large ensemble and the block-bootstrapped ensemble members are generally high, with a median value of 0.65, 0.74 and 0.76 for MIROC6, MPI-ESM1-2-LR and CanESM5 respectively (Figure 3c). These pattern correlations are also substantially higher than those obtained when correlating the uncertainty derived from block-bootstraps of one ensemble member to those from the large ensemble of a different climate model - demonstrating that the bootstrap captures quantitatively different spatial patterns of uncertainty between models (Figure 3d). In particular, all of the 150 individual ensemble members show the highest pattern correlation to their own climate model. We note that for these pattern correlations uncertainty is capped at 100% to avoid the dominance of regions where relative uncertainty diverges due to a very weak anthropogenic signal. Increasing this cap to 200% roughly decreases the values shown in Figure 3c by 0.1.

These results are derived with a bootstrap block width of 5 years, based on a conservative choice to capture all significant autocorrelation seen in the residuals between global temperatures and temperature extremes (Figures A2-4). We note that shorter block widths perform almost equivalently well in terms of reproducing the uncertainty from the large ensemble, with only minor under-estimation of uncertainty when using a block width of only 1 year (i.e. a normal bootstrap) (Figure A5). Using larger block widths - such as 10 years (Figure A6) - substantially reduces the ability of the bootstrap to reproduce both the patterns and magnitude of uncertainty seen in the large ensemble. The results so far described pertain to the frequency of exposure to temperature extremes ($T99p$). We note that very similar results are obtained for the intensity of temperature extremes ($T5dx$), as presented in Figures A7 and A8.



File generated with AMS Word template 2.0

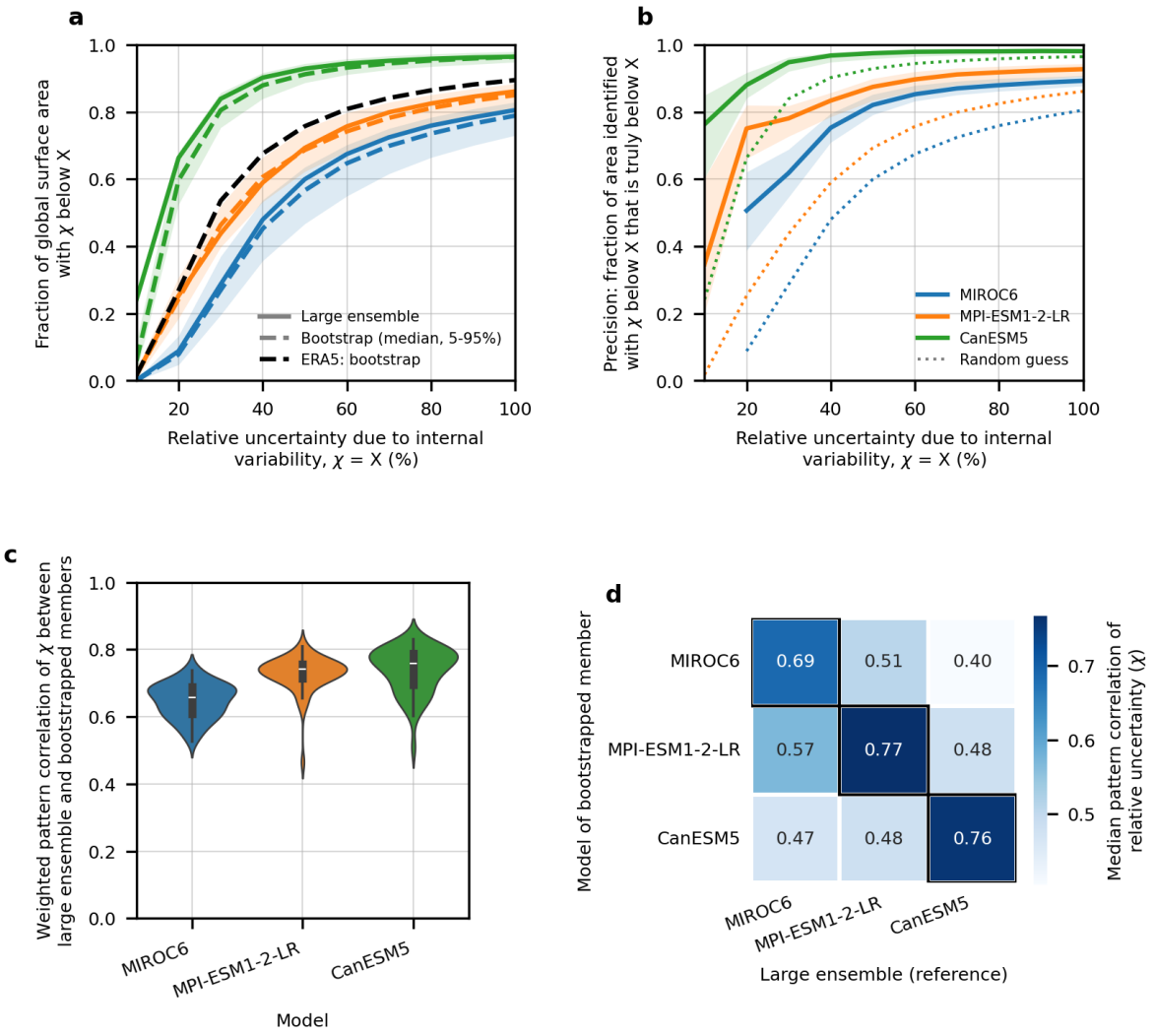



***Figure 3. Comparing uncertainty in temperature extreme frequency attribution between the large ensemble and the block-bootstrapping of individual ensemble members.*** (a) The cumulative surface area fraction under different levels of relative uncertainty estimated from the large ensemble (solid line) and block-bootstrapped individual ensemble members (median across ensemble members: dashed line, 5-95th percentile range across ensemble members: shaded). Results of applying the same block-bootstrap procedure to the ERA5 historical reanalysis are shown in the black dashed line. (b) The precision with which the block-bootstrap estimates of uncertainty correctly identify a given grid-cell as having uncertainty below a given threshold - taking the uncertainty from the large ensemble as the ground truth (see Methods). Solid curves show the median and shaded areas the 5-95th percentile range across the ensemble members. Dotted lines show the expectation from a random guess with a 50% likelihood. Estimates of precision are restricted to cases where at least 1% of the global surface area is below a certain level of uncertainty within the large ensemble. (c) The distribution of area-weighted pattern correlations between relative uncertainty estimates from the large ensemble and the bootstrapped ensemble members, calculated on each model's native grid with relative uncertainty capped at 100%. Relative uncertainty is for the linear-regression slope between global temperatures and the frequency of temperature extremes as displayed in Figures 1 and 2. (d) The median pattern correlation of relative uncertainty between bootstrapped individual ensemble members and different large ensembles. Uncertainty maps are first regridded to the coarsest climate model grid (CanESM5, see Methods).



File generated with AMS Word template 2.0

*Uncertainty in attribution of precipitation extremes*

Turning our attention to precipitation extremes, we note that for the examples selected in Figure 1, local precipitation extremes can show even more diverse relationships with global temperatures due to different realisations of internal variability. When quantifying this contribution globally, we see much larger relative uncertainty compared to temperature (Figure 4, noting the colour scale now extending to 200% rather than 100% as in Figure 2). Relative uncertainty within the large ensemble exceeds 100% for approximately 90%, 75% and 55% of the global surface area in the MIROC6, MPI-ESM1-2-LR and CanESM5 models respectively (Figure 5a). We note that these substantially higher levels of relative uncertainty compared to temperature extremes are to be expected given the much stronger role of internal variability compared to human forcing for precipitation (Deser et al. 2012). The patterns of uncertainty are also distinct across climate models, although lower uncertainty is observed across central Africa and Northern mid-to-high latitudes in all three models.

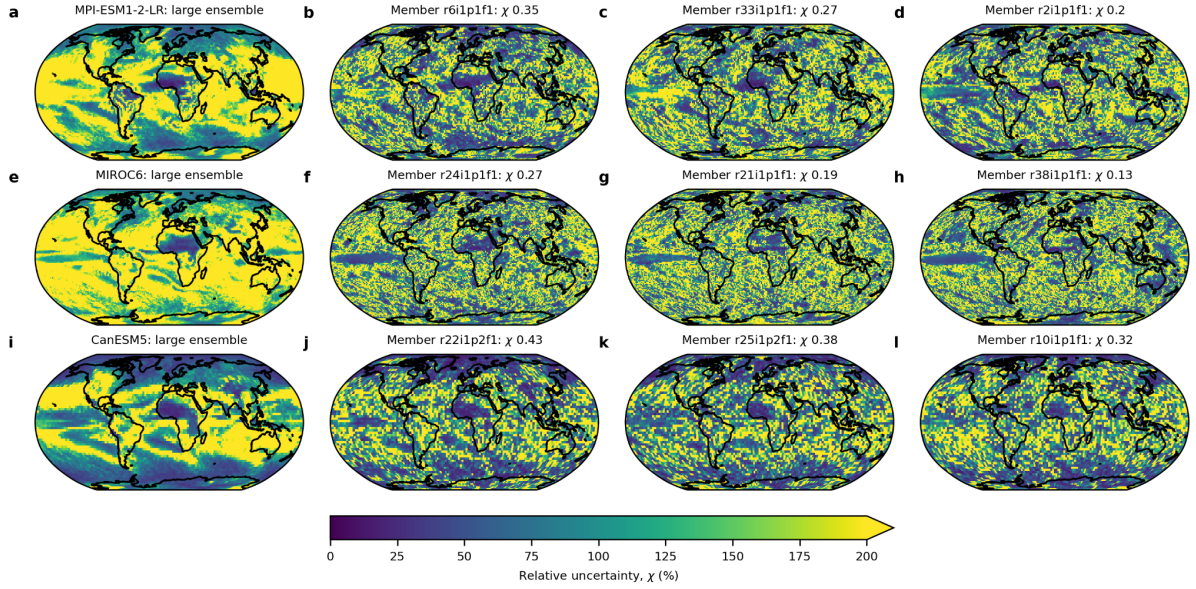



***Figure 4. Relative uncertainty in attribution of precipitation extreme frequency due to internal variability in the large ensembles and block-bootstrapping of individual ensemble members.*** The relative uncertainty (ratio of standard deviation to the mean, χ) of the linear-regression slope between global temperatures and the frequency of precipitation extremes, *P99p*, estimated from the large ensemble (left column). The relative uncertainty estimated by block-bootstrapping individual ensemble members (right columns), for the member with the best, median and worst pattern correlation compared to the uncertainty derived from the large ensemble (respectively left to right). Results are shown for the MPI-ESM1-2-LR (top row), MIROC6 (second row) and CanESM5 (lower row) models.

Investigating the capacity of the block-bootstrap to capture these relative uncertainties within individual ensemble members, we find that it performs considerably worse for precipitation



File generated with AMS Word template 2.0

than for temperature extremes. Bootstrapped estimates show extensive small-scale spatial variability which is not present in the large ensemble (Figure 4), relative uncertainty is typically underestimated by a substantial margin (Figure 5a), and pattern correlations with the large ensemble relative uncertainty are low (median 0.19–0.38 across models, Figure 5b). Since relative uncertainty is the ratio of the standard deviation of the linear-regression slope to its mean, this discrepancy may arise from either component. The absolute uncertainty (the standard deviation, without dividing by the mean) estimated by the bootstrap agrees closely with that of the large ensemble's absolute uncertainty (Figure 6). Pattern correlations of absolute uncertainty with the large ensemble are comparable for precipitation and temperature extremes (Figure 5b), and they reflect quantitatively meaningful differences between climate models: in all 150 bootstrapped ensemble members, the absolute uncertainty derived via bootstrapping correlates most strongly with that from the correct model's large ensemble (Figure 5c). The discrepancy therefore arises from the denominator: the slope estimated from a single ensemble member deviates substantially from the large-ensemble mean, particularly at small spatial scales (Figure A9).

In other words, the bootstrap accurately captures the absolute uncertainty due to internal variability, but where the forced signal is weak, the slope estimated from a single realisation is itself dominated by internal variability, and dividing by it biases the relative uncertainty low. This behaviour is common to all metrics: across grid-cells and climate models, bootstrapped and large-ensemble relative uncertainty agree without systematic bias up to levels of around 100% for both temperature and precipitation extremes, with the bootstrap estimates saturating at approximately 150% beyond this (Figure 5d). This saturation matches the theoretical expectation for cases where the signal to noise ratio approaches zero (see Appendix B). Precipitation extremes therefore do not behave differently from temperature extremes in this respect; they simply occupy the high end of the relative uncertainty range where the forced signal is still small compared to the noise from internal variability. Equivalent analysis for the intensity of precipitation extremes (P5dx) shows very similar results (Figure 5b, d; Figures A10, A11).



File generated with AMS Word template 2.0

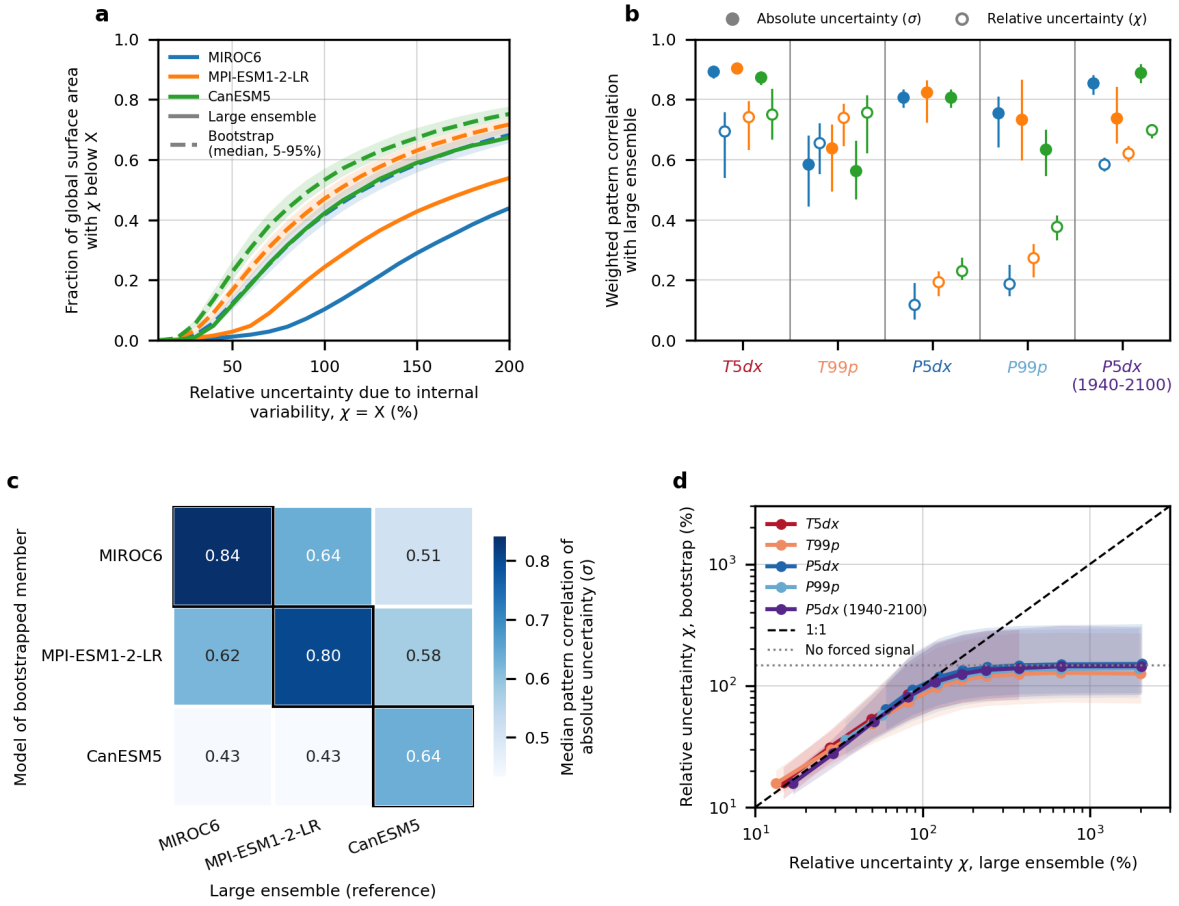



***Figure 5. Relative and absolute uncertainty in bootstrap attribution for temperature and precipitation extremes.*** (a) The cumulative surface area fraction under different levels of relative uncertainty estimated from the true ensemble (solid line) and bootstrapped ensemble members (median across ensemble members: dashed line, 5-95th percentile range: shaded) for heavy precipitation extreme frequency, *P99p*. Note the extended x-axis scale compared to Figure 3a. (b) Area-weighted pattern correlations of absolute (filled circles) and relative (open circles) uncertainty between the true ensemble and the bootstrapped ensemble members, showing the median (circles) and 5-95th percentile range (bars) across ensemble members for each model. Uncertainty is for the linear-regression slope between global temperatures and local extremes, shown for all climate metrics for comparison, including *P5dx* over 1940-2100 using forcing from SSP5-8.5 from 2015. (c) The median pattern correlation of absolute uncertainty for precipitation extreme frequency, *P99p*, between bootstrapped individual ensemble members and different large ensembles. Uncertainty maps are first regridded to the coarsest climate model grid (CanESM5). (d) The scaling of relative uncertainty estimated from the bootstrap with that estimated from the large ensemble across climate extreme metrics. Solid lines show the median, and shaded area the interquartile range, estimated across grid-cells, ensemble members and climate models (area-weighted) for different binned levels of the relative uncertainty derived from the large ensemble, showing only bins which cover at least 1% of the global surface area. Dashed black shows the 1:1 line and dotted grey the theoretically expected relative uncertainty in a case where the signal-to-noise ratio approaches zero (100/0.674 ≈ 148%; Appendix B).



File generated with AMS Word template 2.0

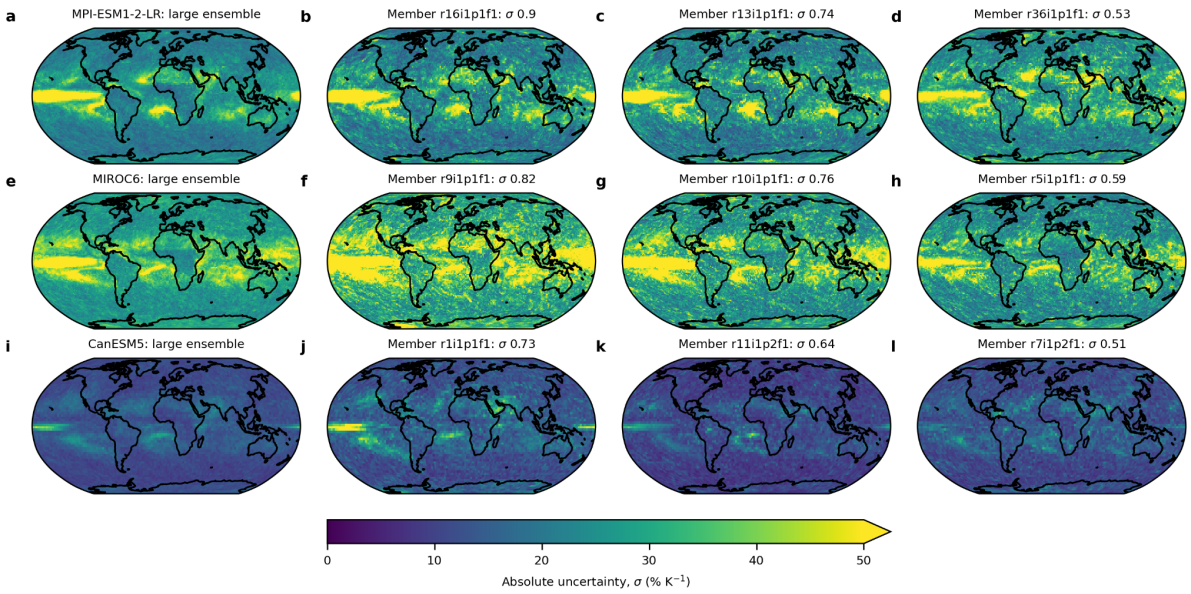



***Figure 6. Absolute uncertainty in attribution of precipitation extreme frequency due to internal variability in the large ensembles and block-bootstrapping of individual ensemble members.*** The absolute uncertainty (standard deviation, σ) of the linear-regression slope between global temperatures and the frequency of precipitation extremes, *P99p*, estimated from the large ensemble (left column). The absolute uncertainty estimated by block-bootstrapping individual ensemble members (right columns), for the member with the best, median and worst pattern correlation compared to the uncertainty derived from the large ensemble (respectively left to right). Results are shown for the MPI-ESM1-2-LR (top row), MIROC6 (second row) and CanESM5 (lower row) models.

We explore two ways in which enhancing the strength of the signal-to-noise ratio could yield better representation of the relative uncertainty by the bootstrap approach for precipitation extremes. First, by block-averaging adjacent grid cells to spatial scales of 5 or 10 degrees, the signal-to-noise ratio is increased by reducing noise (Fischer et al. 2013). While this brings reductions in the general levels of relative uncertainty and a better comparison between the bootstrap and large ensemble, some bias remains and pattern correlations remain lower than for temperature extremes (Figures A12 & A13). Second, under an extended time-series to 2100 with strong anthropogenic forcing (SSP5-8.5), the forced signal is stronger than at present-day, and therefore levels of relative uncertainty are much lower across most of the global surface area except in regions with strong dynamical contributions to precipitation decline (Pfahl et al. 2017) (Figure A14). In this latter case, bootstrap estimates no longer under-estimate the levels of relative uncertainty compared to the large ensemble (Figure A15) and their spatial patterns are highly similar, as in the case of temperature extremes (Figure 5b). This demonstrates that with a stronger forced signal, estimates of the relative



File generated with AMS Word template 2.0

uncertainty of the linear-regression slope of precipitation extremes with GMST also become accurate with the bootstrap approach.

*Practical recommendations on application to observations*

Given the difference in performance of the block-bootstrap for absolute and relative uncertainty when the signal-to-noise ratio is low, as found for precipitation extremes, we make a number of practical recommendations for its application to single realisations such as observations. The close agreement between the absolute uncertainty estimated by bootstrapping and that of the large ensembles implies that confidence intervals on the GMST-regression slope estimated from a single realisation can be trusted to represent the uncertainty arising from internal variability. Indeed, across grid-cells and climate models, confidence intervals from bootstrapping individual ensemble members contain the true forced response (the large-ensemble mean) close to the nominal fraction of the time (Figure A16a). The slight under-coverage of a few percentage points for all climate metrics (e.g. 84–88% for nominal 90% intervals) likely reflects a modest underestimation of sampling variability by the bootstrap, as 5-year blocks cannot retain all variability, particularly that on multi-decadal timescales (while noting that increasing block-widths reduces performance due to insufficient bootstrap samples, Figure A6). This holds for both temperature and precipitation extremes, and we recommend confidence intervals on the GMST-regression slope as the primary use of the bootstrap approach.

By contrast, relative uncertainty from the bootstrap requires more careful interpretation. While it is not systematically biased relative to the large ensemble up to levels of around 100% (Figure 5d), its noise means that a low bootstrapped relative uncertainty does not guarantee a low true relative uncertainty. How reliable it is depends on how common grid-cells with a robust forced signal are. For temperature extremes, where most of the globe has a true relative uncertainty below 100%, a bootstrapped relative uncertainty of 40–50% corresponds to a true (large-ensemble) relative uncertainty below 100% in 88–95% of cases (Figure A16b). For precipitation extremes at current levels of global warming, grid-cells with a robust forced signal are rare. A low bootstrapped relative uncertainty is then frequently a chance outcome in a grid-cell without a robust signal, and the same 40–50% corresponds to a true relative uncertainty below 100% in only 8–62% of cases, depending on metric and



File generated with AMS Word template 2.0

model (Figure A16b). Under stronger forcing (SSP5-8.5 to 2100), precipitation extremes reach confidence levels similar to temperature extremes (Figure A16b). Nevertheless, even at current levels of warming, a bootstrapped relative uncertainty of 40–50% identifies the sign of GMST-regression slope correctly in 78–93% of cases for precipitation extremes, and in 98–99% of cases for temperature extremes (Figure A16c). In practice, we therefore suggest that for temperature extremes a bootstrapped relative uncertainty below ~50% can be taken as indicating a robust, attributable signal. For precipitation extremes at current warming levels, it should be interpreted as evidence for the direction of an attributable signal rather than for its robustness, and values above 100% should be treated as not attributable for both.

*Application to the attribution of real-world changes*

Given the demonstrated skill of the bootstrap approach for quantifying both absolute and relative uncertainty in attribution of temperature extremes with single realisations (Fig. 3), we apply this approach to historical reanalysis data of temperature extreme intensity from ERA5. Patterns of uncertainty in ERA5 (Fig. 7a) show some similarities and distinctions from those identified in the climate model large ensembles (Fig. 2). Uncertainty in the South-East Pacific in ERA5 is substantially lower than the consistently high levels of uncertainty seen in the three climate models. South America and central-Southern Africa show higher uncertainty than the Indo-Pacific and North Africa consistently across both ERA5 and the three climate models. Across the Northern mid-latitudes, Europe shows the lowest levels of relative uncertainty in ERA5 - likely a reflection of the high rate of recent warming observed across the continent. Aggregating spatially, approximately 90% of the global surface area has uncertainty levels below 100% in ERA5, with uncertainty lower than that observed in MIROC6, but substantially higher than in CanESM5, most closely resembling that seen in MPI-ESM1-2-LR (Figure A8).

We choose a set of cities across continents to demonstrate the application of this block-bootstrap approach to generate counterfactuals of temperature extremes in the absence of climate change (see Methods). These demonstrate diverse attribution outcomes at the local level. On the one hand, counterfactuals generated for Madrid and Riyadh indicate that heat extremes are now 2-3C warmer than in a counterfactual in which global temperatures remained at 1940-1970 levels. On the other hand, the counterfactual for Sydney does not show a clear heat intensification signal, and Delhi even shows a weak cooling due to climate change. Importantly, the quantification of uncertainty using the bootstrap approach allows



File generated with AMS Word template 2.0

greater confidence in intermediate cases like Sao Paolo and Jakarta, where the warming signal is less strong but the quantification of counterfactuals and their uncertainties clearly shows the significant role of climate change in intensifying these heat extremes. We note that for heat extremes, regions of large relative uncertainty often reflect those of weak observed trends in temperature extremes, as well as regions of high absolute uncertainty, both in ERA5 and the climate model ensembles (Figure A17).

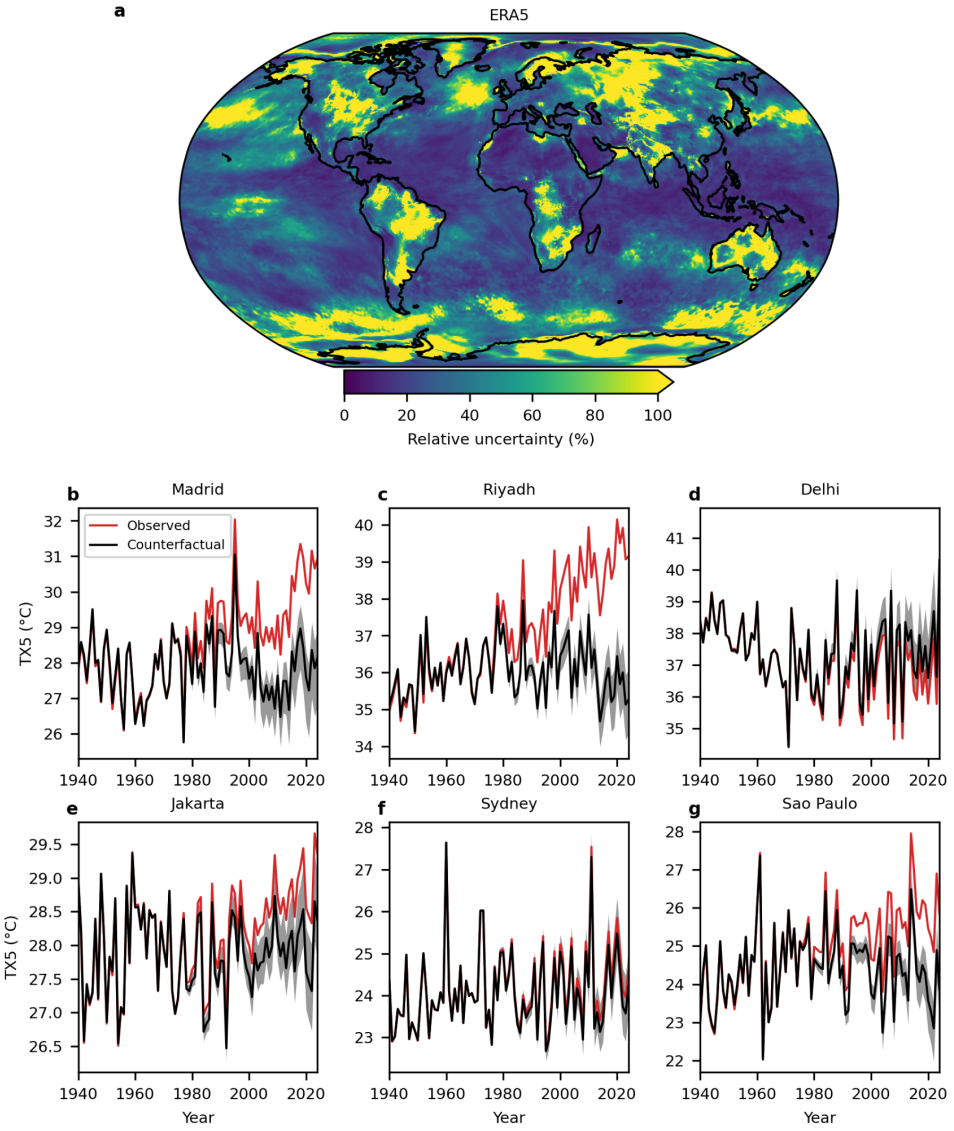



***Figure 7. GMST linear-regression based attribution of heat extremes in the ERA5 reanalysis.*** (a) The relative uncertainty in the linear-regression slope between global mean surface temperature (GMST) and the annual hottest five days (T5dx) over 1940-2025. (b-g) Attribution of observed changes in T5dx (red) from 6 example cities, using the GMST linear-regression slopes to derive counterfactual scenarios (black) in the absence of further climate change since 1940-1970. 95% confidence intervals for the counterfactuals are shown in shaded grey obtained from the block-bootstrapping procedure.



File generated with AMS Word template 2.0

## 4 Discussion

To confidently attribute changes in extremes and their impacts to anthropogenic climate change one must be clear that they would have been unlikely to occur due to internal climate variability alone. Our work provides a formalised framework in which to assess whether approaches for attribution from a single realisation using linear-regression with GMST currently meet this criteria (Mengel et al. 2021; Dimitrova et al. 2024; Beck et al. 2024; Kotz et al. 2025), and whether improvements may enable them to do so.

Our first contribution is to show that internal variability contributes substantial uncertainties to these attribution approaches, generating relative uncertainties exceeding 100% across large parts of Earth, even for temperature extremes. For precipitation extremes, the contribution of internal variability is much larger, and both examples make the case that internal variability should be considered in these approaches to ensure robust uncertainty estimates for climate attribution statements. Approaches to attribution using only observations which do not capture this source of uncertainty (Mengel et al. 2021) likely over-state confidence of attribution to human influence, particularly for heavy precipitation extremes.

However, our second contribution is to show that robust uncertainty estimates can be derived for observationally-based attribution of climate extremes. The block-bootstrap approach is easy to implement and provides estimates of absolute uncertainty on the GMST linear regression slope which closely match those of a large ensemble, with confidence intervals that contain the large ensemble mean close to their nominal rate for both temperature and precipitation extremes. Researchers aiming to attribute changes in regional climate extremes and their impacts to global warming may therefore work with observations rather than climate models, benefiting from lower computational costs and avoiding model biases in the forced response, while still obtaining attribution statements which capture the uncertainty associated with internal variability. Relative uncertainty requires more care: because it divides by the slope estimated from a single realisation, it becomes unreliable where the forced signal is weak relative to internal variability, as is the case for heavy precipitation extremes at current levels of anthropogenic forcing. Where the true relative uncertainty exceeds ~100%, bootstrapped estimates are biased low, and a low bootstrapped relative uncertainty is more often a chance outcome. By averaging out noise, aggregation of



File generated with AMS Word template 2.0

precipitation extremes to larger spatial scales strengthens the signal-to-noise ratio and partially alleviates this, while under stronger forcing (SSP5-8.5 by the end of the century) the bootstrap approach to attribution for precipitation extremes reaches an accuracy in the relative uncertainty equivalent to temperature extremes. In practice, this means that bootstrapped confidence intervals should form the primary basis for attribution statements, with relative uncertainty interpreted cautiously where forced signals are weak (see the practical recommendations in Section 3).

An important limitation of our work is that we considered only high temperature and heavy precipitation extremes. While this choice was necessary to contain the scope of our analysis and to focus on impact-relevant variables, other climate variables may exhibit different behaviour. The strong consistency between the frequency and intensity of different climate extremes (an overview shown in Figure 5b and 5d) indicates that some generalities may exist. We also expect that for other variables with weak signal-to-noise ratios at current levels of global warming - e.g. wind speed - estimates of relative uncertainty will likely be biased and researchers should follow the advice given for precipitation outlined above.

Our study has focussed on the application of this approach to observationally-derived attribution statements (Mengel et al. 2021), and it is worth commenting on areas in which climate models can still play an important role in attribution. First, where the forced signal is weak relative to internal variability, a single observational record may simply be insufficient to establish a robust attribution, even with well-calibrated absolute uncertainty estimates (Figures 5d, A17). This is particularly relevant for precipitation extremes at current levels of global warming, and potentially for other variables with weak signal-to-noise ratios. In these cases, model-based detection and attribution approaches, which combine observations with simulated fingerprints of the forced response across larger spatial scales, remain a key source of attribution statements. For precipitation extremes, these provide a good degree of confidence in observed changes attributable to human influence across most regions at larger spatial scales (Arias et al. 2021; Paik et al. 2020). Second, observational approaches using linear regression on GMST are unable to resolve individual anthropogenic forcings such as greenhouse gases versus aerosols (Mengel et al. 2021). Climate models will therefore also remain crucial for quantifying these different anthropogenic contributions, which may confound one another when using observations alone.



File generated with AMS Word template 2.0

By establishing an approach which can provide robust uncertainty estimates for attribution of climate extremes using observations alone, our paper brings these methods to a closer point of comparison to climate models. This will allow for a better integration of the complementary strengths of observational and climate model-based attribution approaches, as well as for greater confidence in the attribution of regional heat extremes and their impacts when using observations alone.



File generated with AMS Word template 2.0

*Data Availability Statement.*

Temperature and precipitation data from ERA5 are publicly available from Copernicus (https://cds.climate.copernicus.eu/datasets/reanalysis-era5-single-levels?tab=overview ). Temperature and precipitation data from the three CMIP6 models used are available publicly from the Earth System Grid Federation ( https://esgf.github.io/). Code for the analysis is available at: https://github.com/maxkotz17/GMT_attribution_large_ensemble_tests . Processed data is stored on the HPC infrastructure of the Barcelona Supercomputing Centre and can be shared upon request.

*Acknowledgements*

The authors have no competing interests to declare. MK gratefully acknowledges the support of the European Union's Horizon 2020 research and innovation programme under the Marie Skłodowska-Curie grant agreement no. 101148359. MGD acknowledges support by the Horizon Europe project EXPECT (Grant 101137656).

# APPENDIX A

## Additional figures

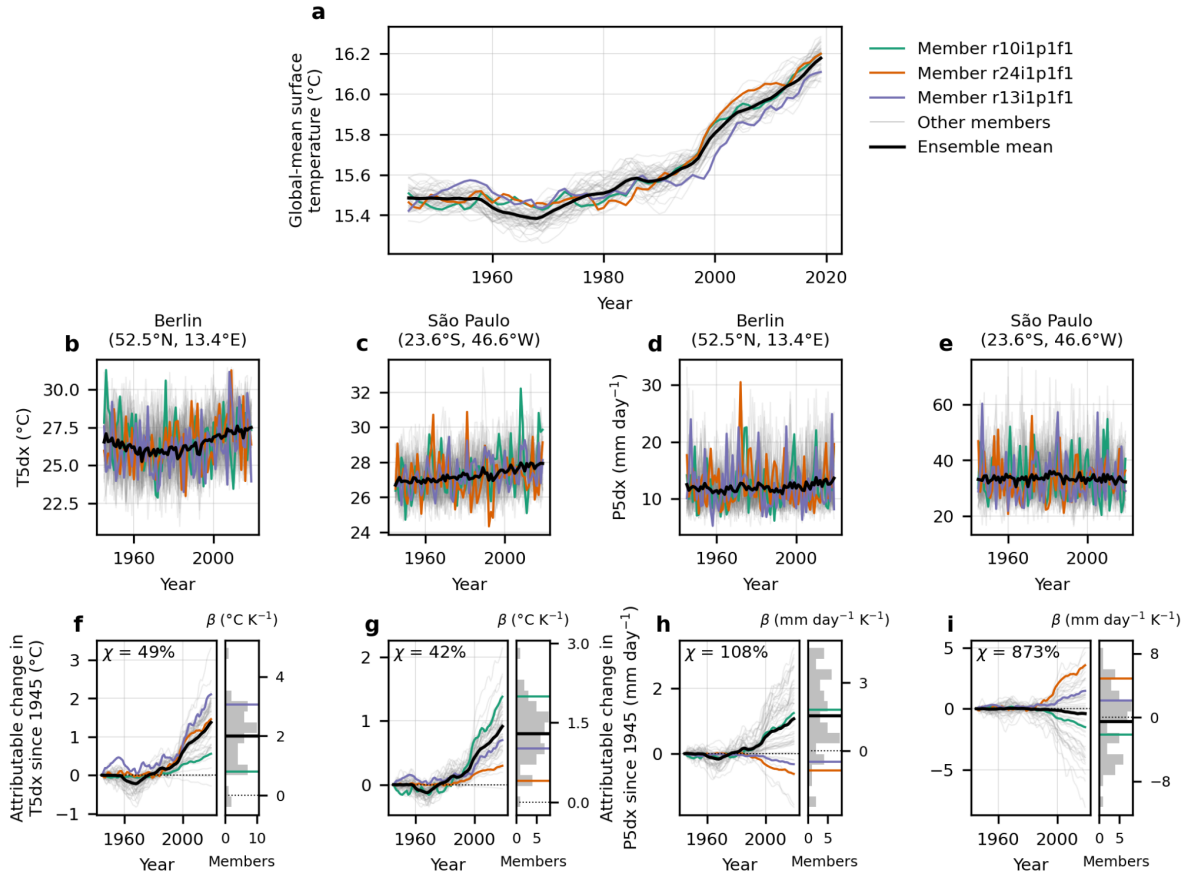



***Figure A1. Internal variability generates diverse relationships between global temperature and local climate extreme intensity.*** The structure of the Figure is the same as Figure 1, but results are shown for the intensity of climate extremes, based on the annual maximum of 5 day average of daily surface temperature and precipitation ("T5dx" and "P5dx").



File generated with AMS Word template 2.0

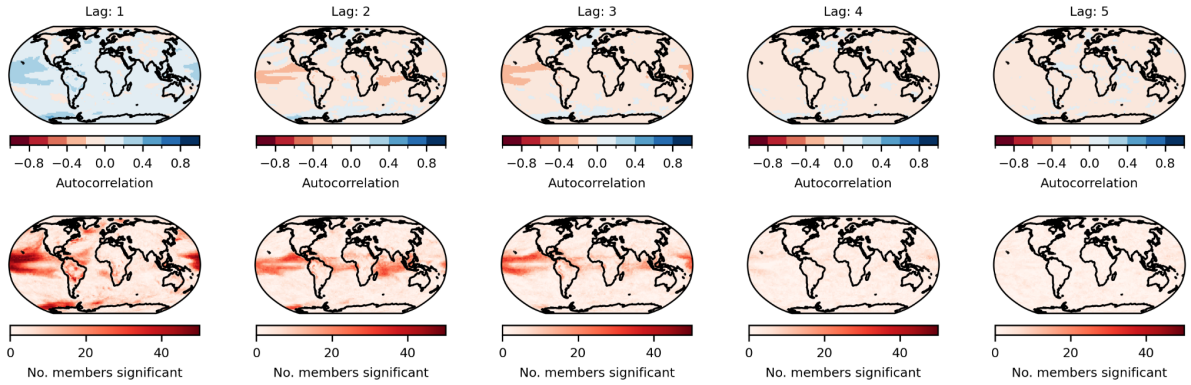



**Fig. A2. Autocorrelation of the residuals of the global temperature to extreme frequency (T99p) regression.** The upper row shows the autocorrelation values, averaged across ensemble members of MPI-ESM1-2-LR. The lower row shows the number of ensemble members with autocorrelation values which are significant at the 5% level based on a two-sided significance test. Uncertainty in the autocorrelation values are calculated based on the Bartlett formula.

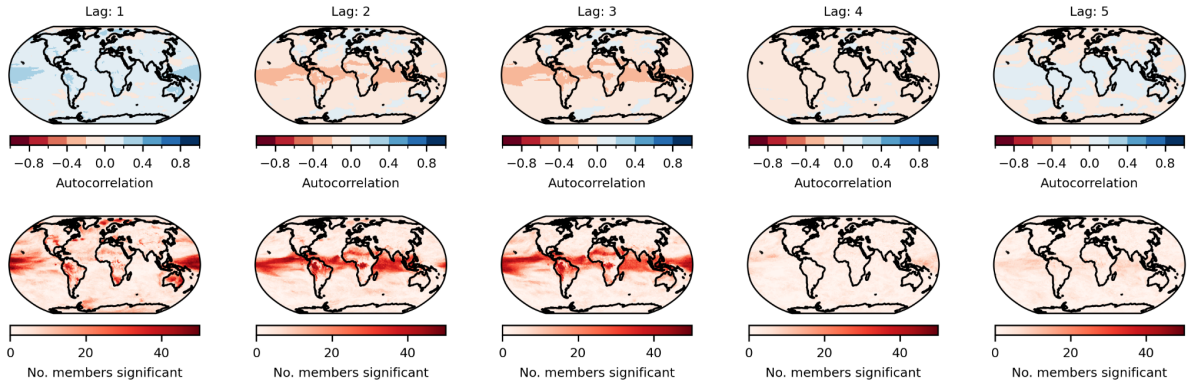



***Fig. A3. Autocorrelation of the residuals of the global temperature to local extreme frequency (T99p) regression for the MIROC6 model.*** Details as in Fig. A2.

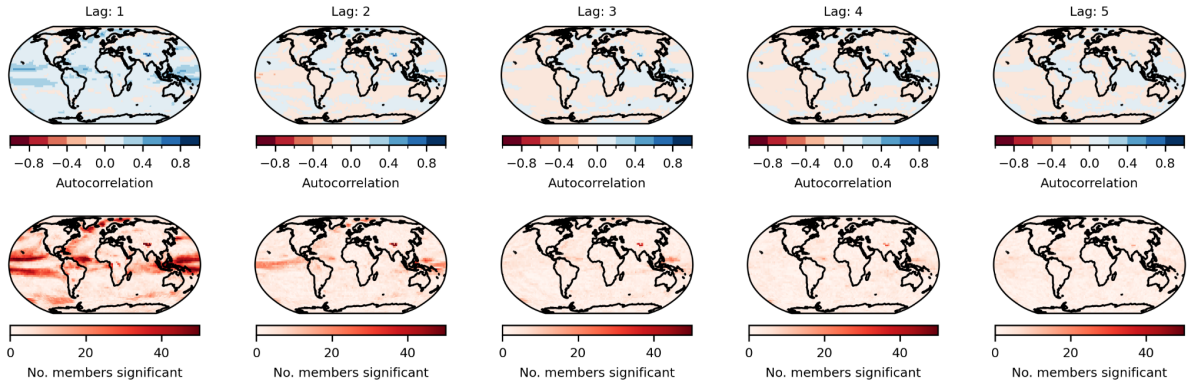
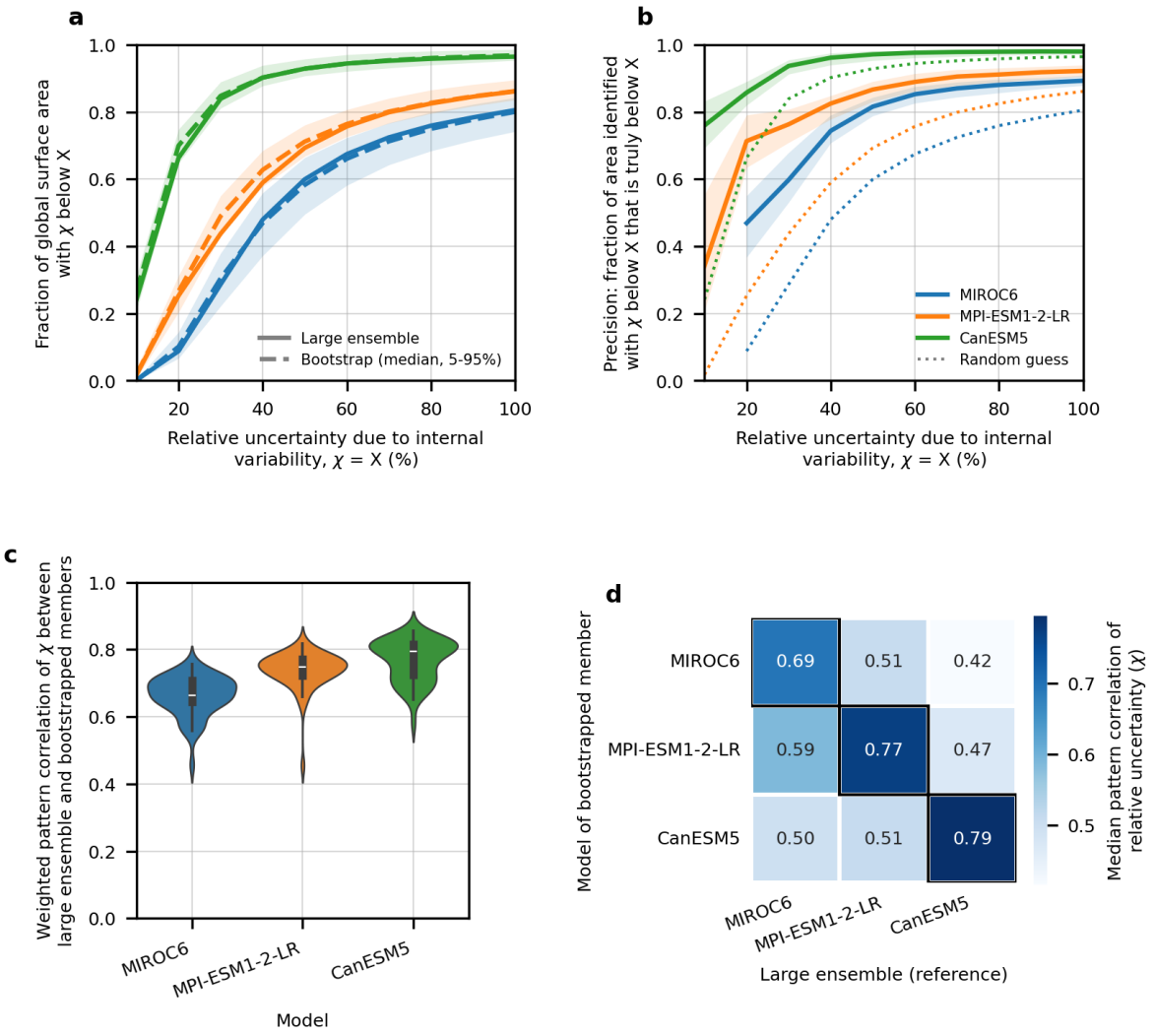



***Fig. A4. Autocorrelation of the residuals of the global temperature to local extreme frequency (T99p) regression for the CanESM5 model.*** Details as in Fig. A2.



File generated with AMS Word template 2.0




734

735 ***Figure A5. Uncertainty in temperature extreme frequency (T99p) attribution when using a***
736 ***block-bootstrap with block width of 1 year.*** Figure is otherwise as Figure 3.
737

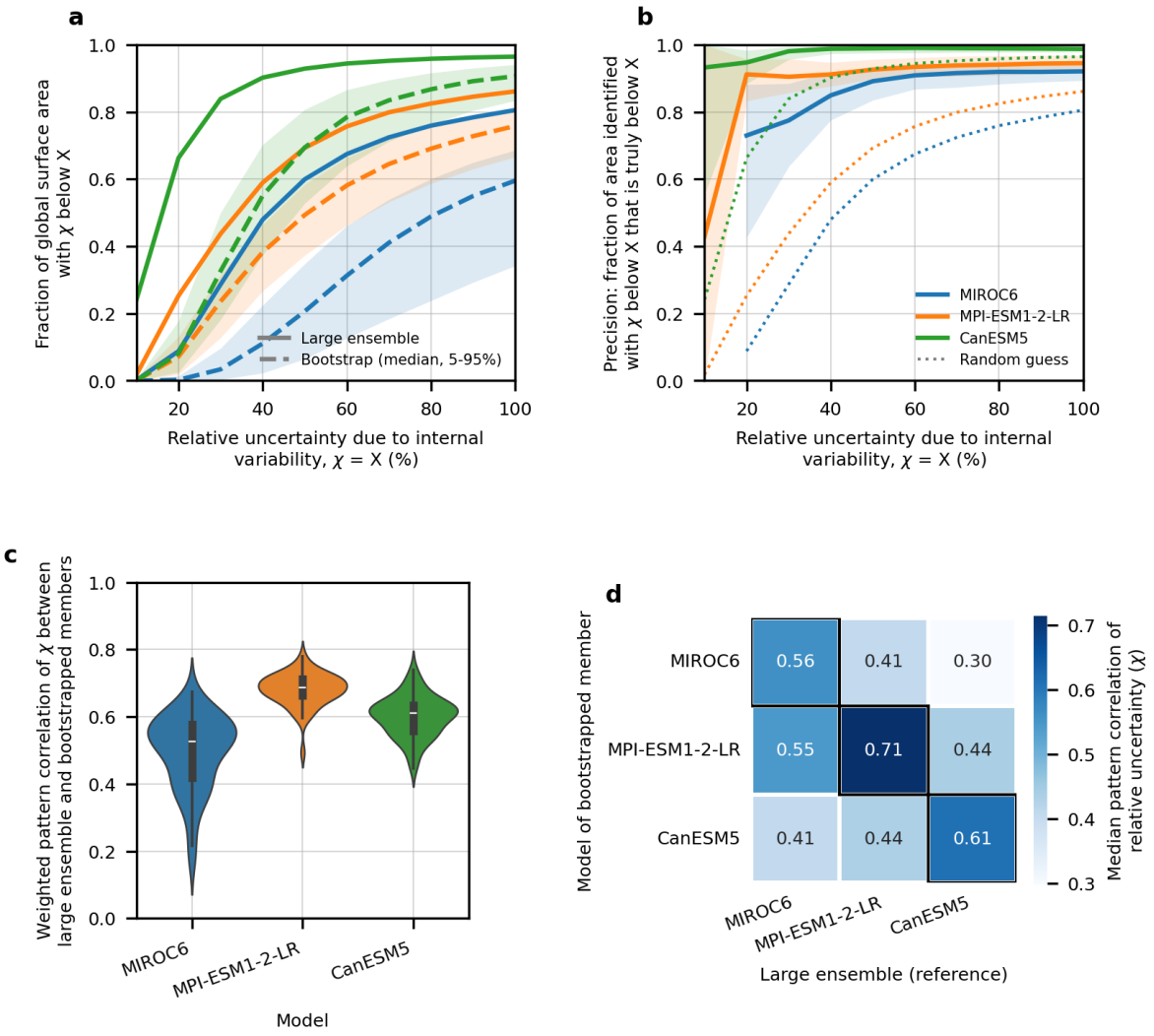



***Figure A6. Uncertainty in temperature extreme frequency (T99p) attribution when using a block-bootstrap with block width of 10 years.*** Figure is otherwise as Figure 3.

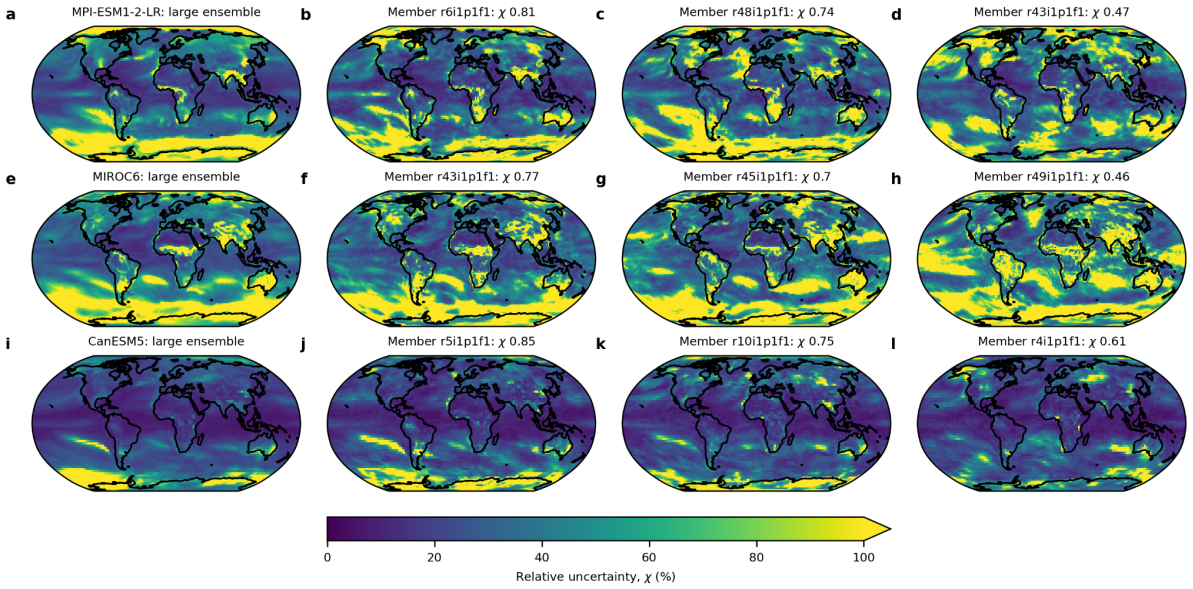



***Figure A7. Relative uncertainty in temperature extreme intensity attribution due to internal variability; as reflected in large ensembles and block-bootstrapping of individual ensemble members.*** As Figure 2 of the main manuscript but for the intensity metric $T5dx$. Results are shown for a block width of 5, based on an assessment of the autocorrelation of residuals as outlined in the manuscript.



File generated with AMS Word template 2.0

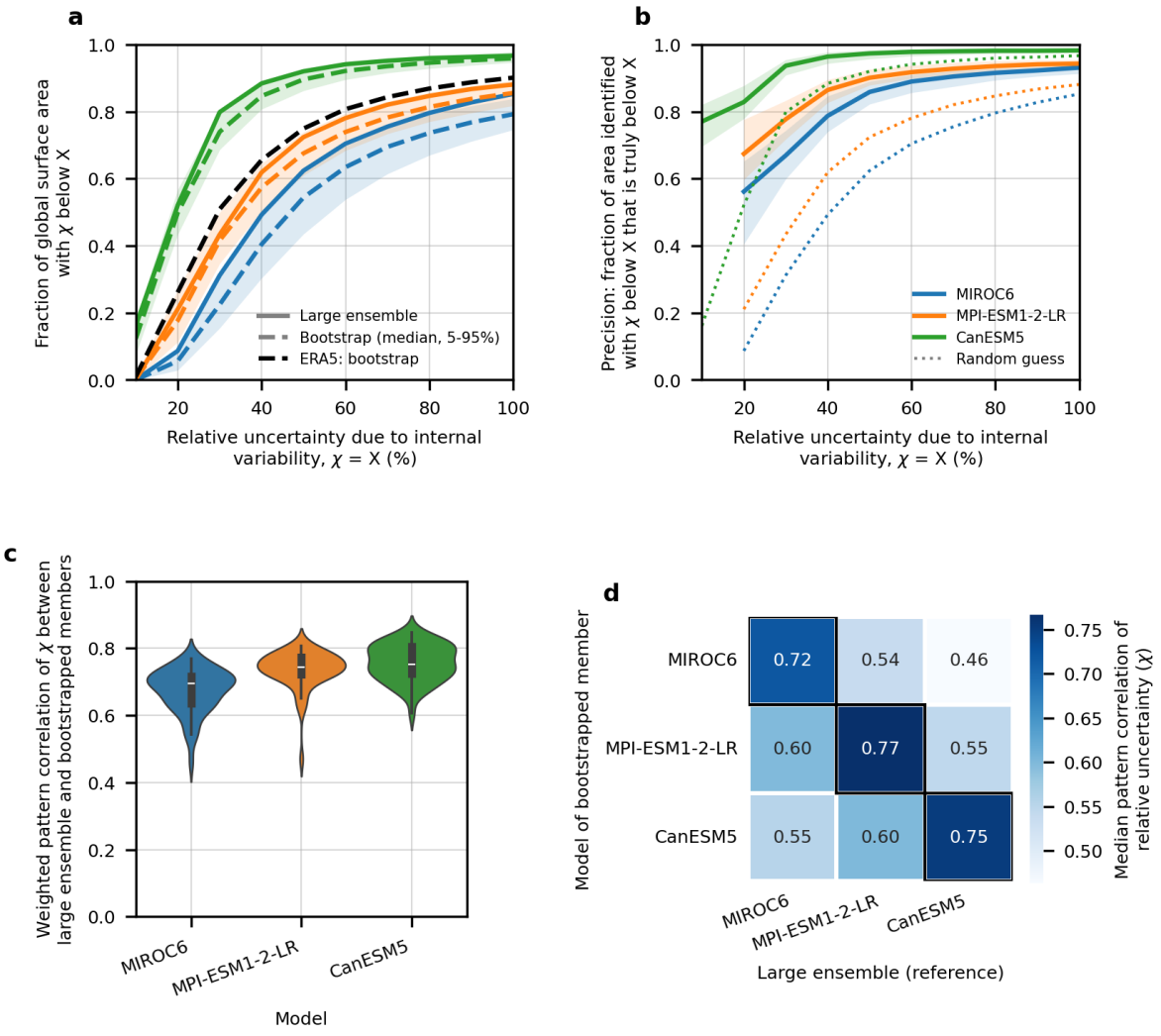



***Figure A8. Comparing uncertainty in temperature extreme intensity attribution between the large ensemble and the block-bootstrapping of individual ensemble members.*** As Figure 3 of the main manuscript but for the temperature extreme intensity metric $T5dx$.



File generated with AMS Word template 2.0

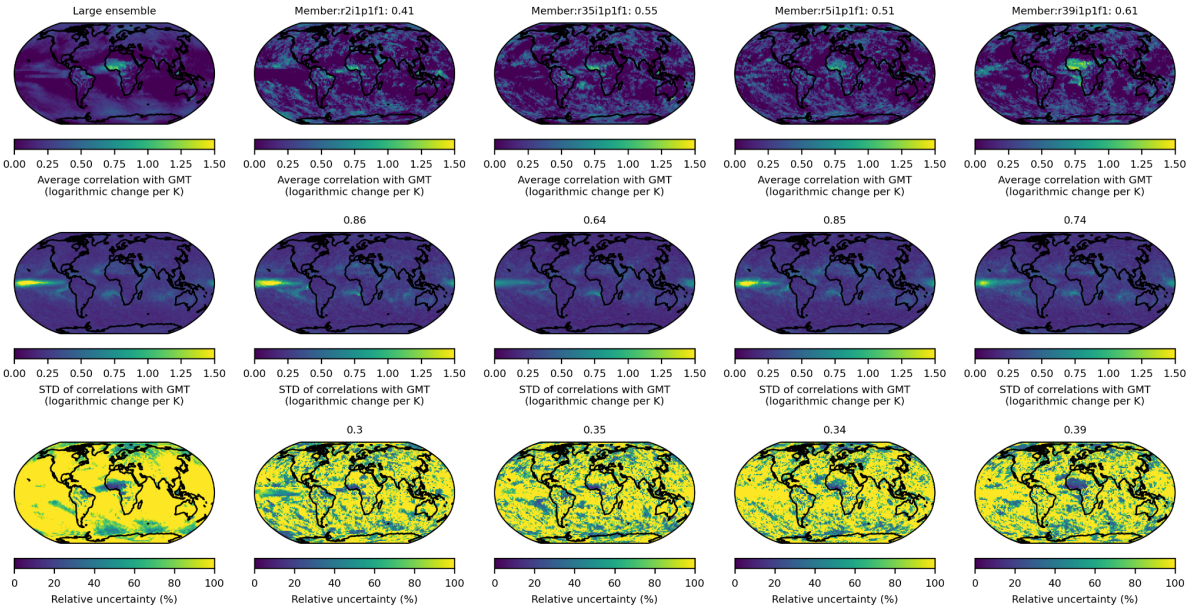



***Figure A9. Composition of relative uncertainty for precipitation extreme frequency (P99p) in the large ensemble and block-bootstrap approaches.*** Average (upper row), standard deviation (second row), and relative uncertainties (lower row) of the linear-regression slope between global temperatures and precipitation extremes. Estimates from the MPI-ESM1-2-LR true large ensemble (left column) and for four examples of individual ensemble members to which the block-bootstrap procedure has been applied.

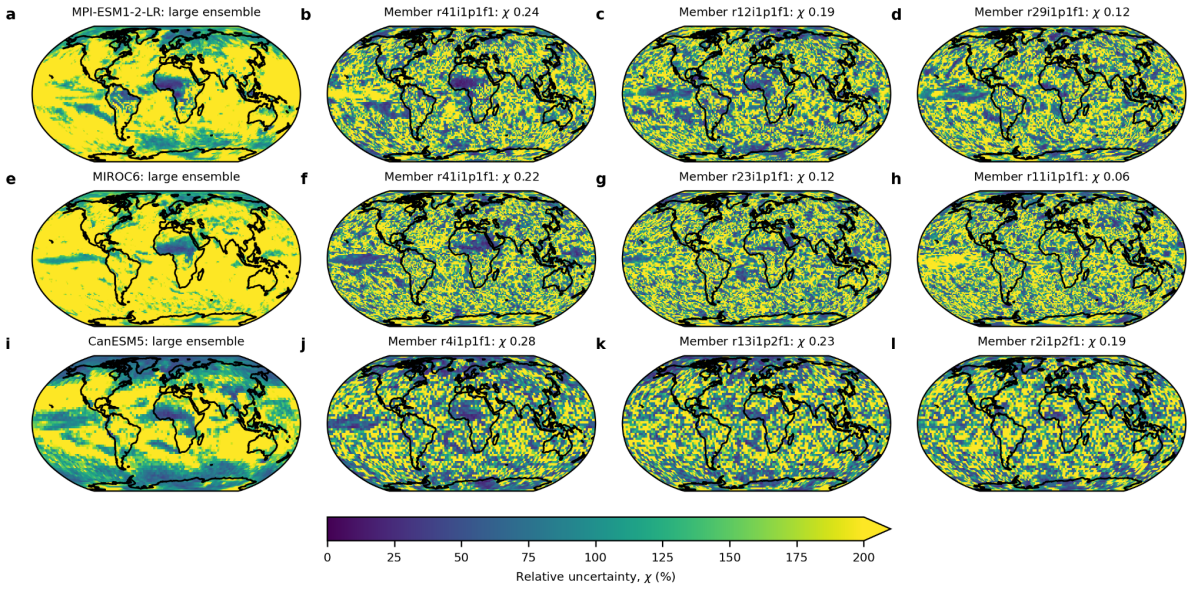



***Figure A10. Relative uncertainty in precipitation extreme intensity attribution due to internal variability; as reflected in large ensembles and block-bootstrapping of individual ensemble members.*** As Figure 4 of the main manuscript but for the intensity metric $P5dx$. Results are shown for a block width of 5, based on an assessment of the autocorrelation of residuals as outlined in the manuscript.



File generated with AMS Word template 2.0

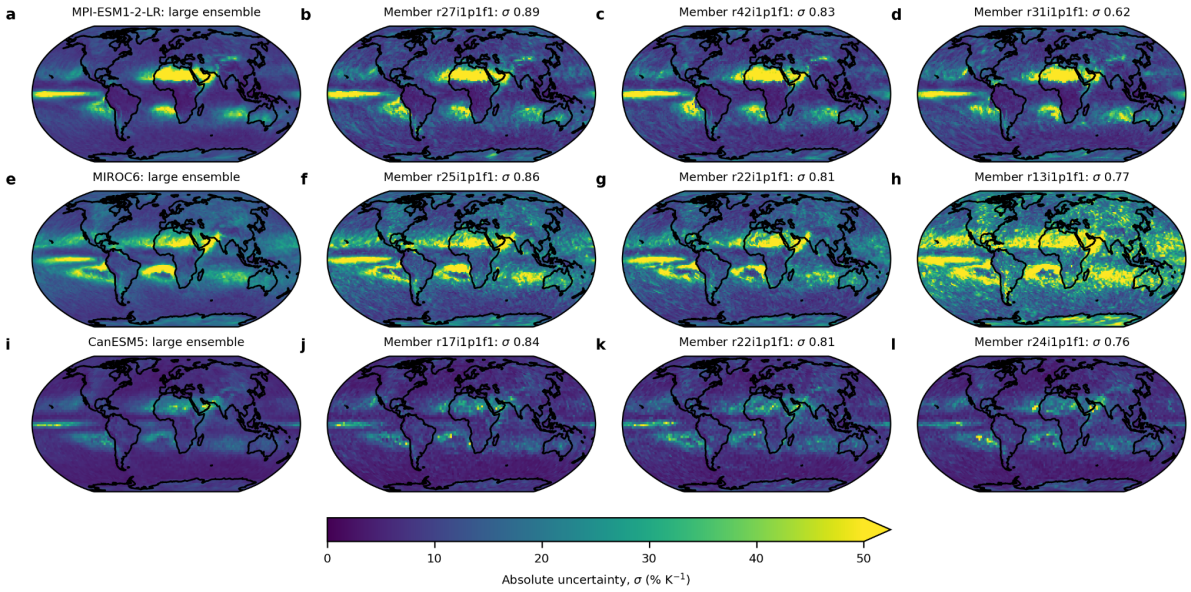



***Figure A11. Absolute uncertainty in precipitation extreme intensity attribution due to internal variability; as reflected in large ensembles and block-bootstrapping of individual ensemble members.*** As Figure 6 of the main manuscript but for the intensity metric $P5dx$. Results are shown for a block width of 5, based on an assessment of the autocorrelation of residuals as outlined in the manuscript.



File generated with AMS Word template 2.0

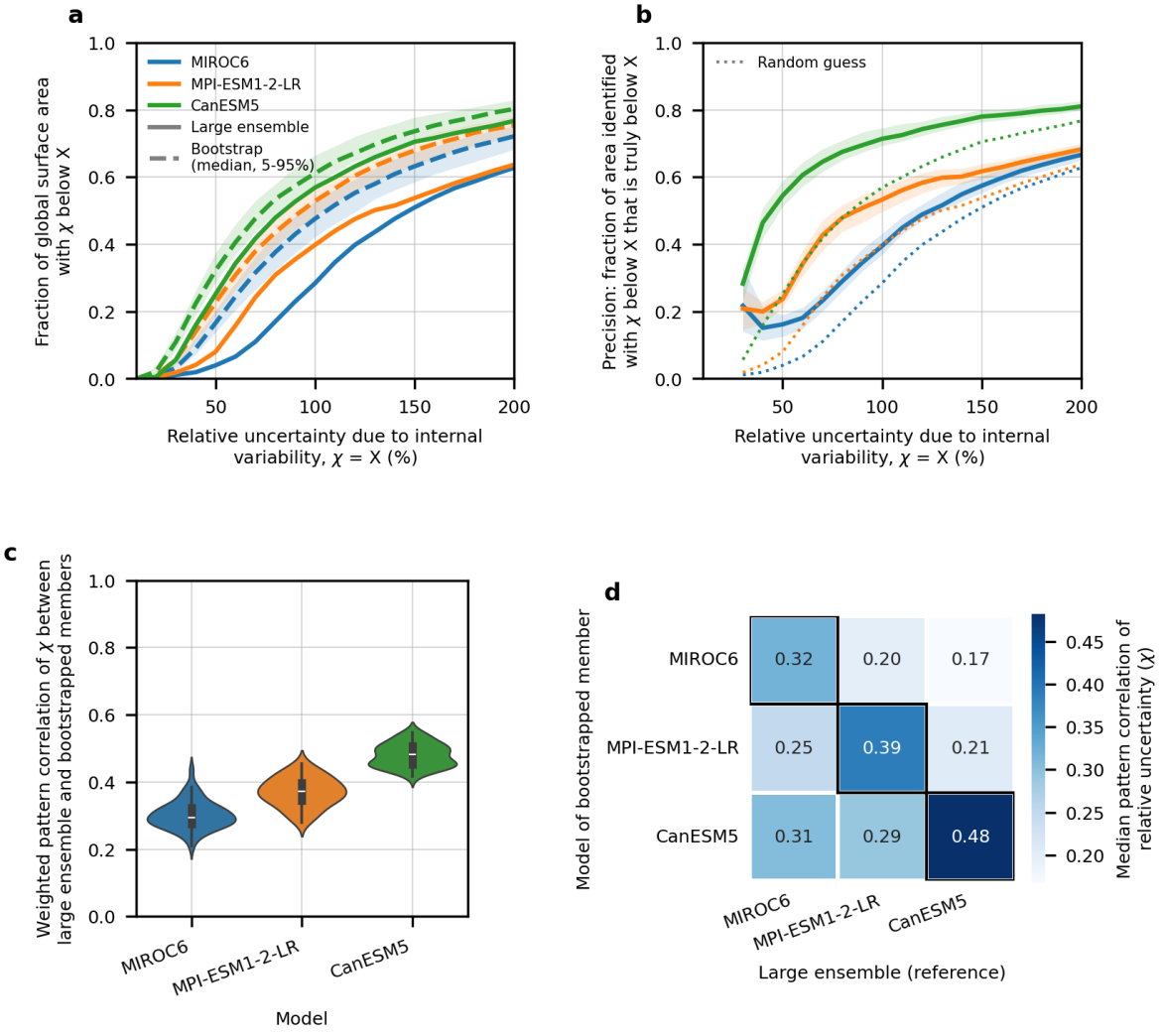



***Figure A12. Comparing uncertainty in precipitation extreme frequency attribution when using spatial aggregation.*** As Figure 3 of the main manuscript but for heavy precipitation extreme frequency, *P99p*, having first aggregated the metric to approximately five degree grid-cells. We average climate extremes over $N$ adjacent grid-cells where $N \approx \frac{5}{r}$ (with $r$ the native model resolution) before applying the attribution and other analytical procedures.



File generated with AMS Word template 2.0

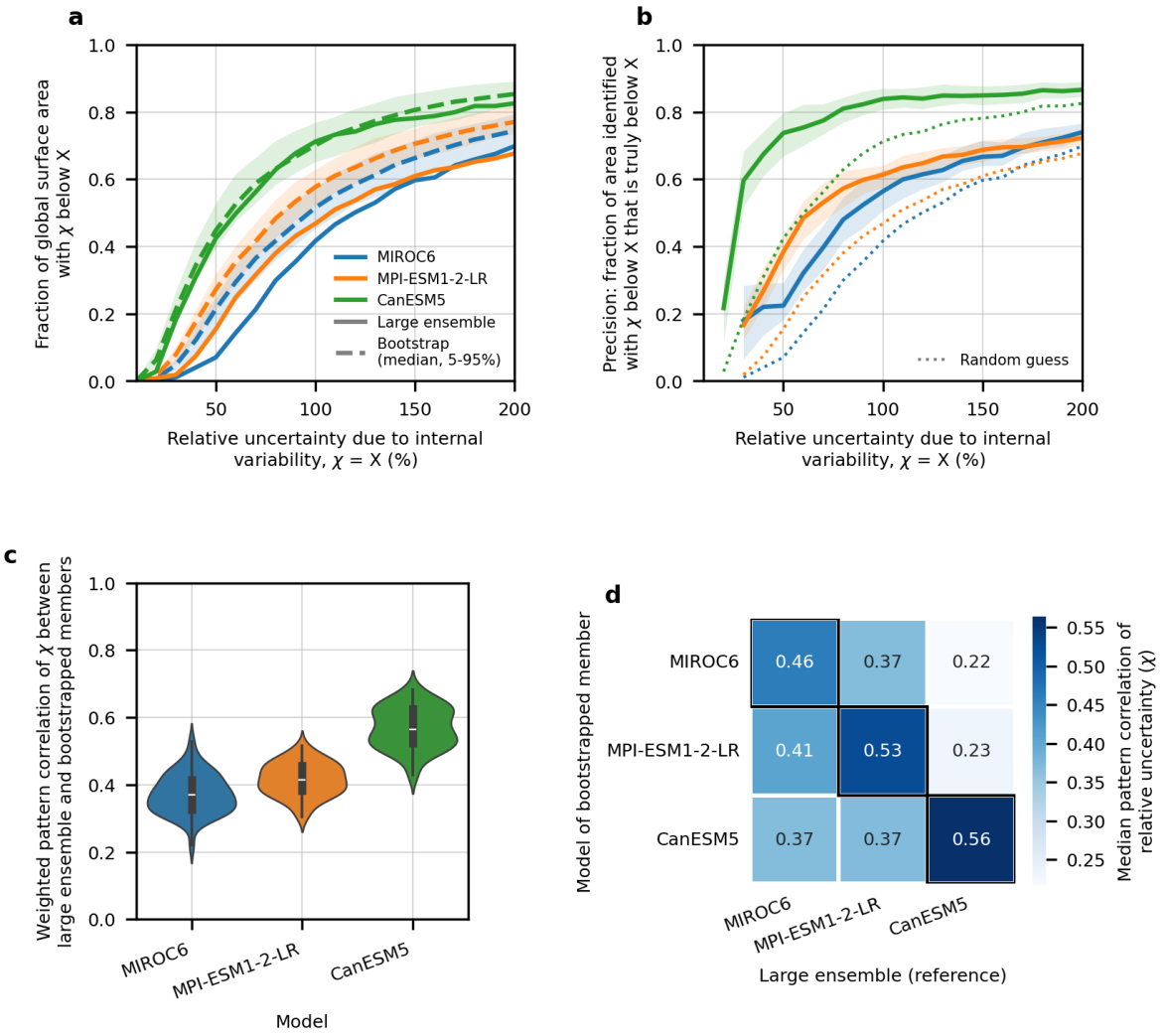



***Figure A13. Comparing uncertainty in precipitation extreme frequency attribution when using spatial aggregation.*** As Figure 3 of the main manuscript but for heavy precipitation extreme frequency, *P99p*, having first aggregated the metric to approximately ten (lower) degree grid-cells. We average climate extremes over $N$ adjacent grid-cells where $N \approx \frac{10}{r}$ (with $r$ the native model resolution) before applying the attribution and other analytical procedures.



File generated with AMS Word template 2.0

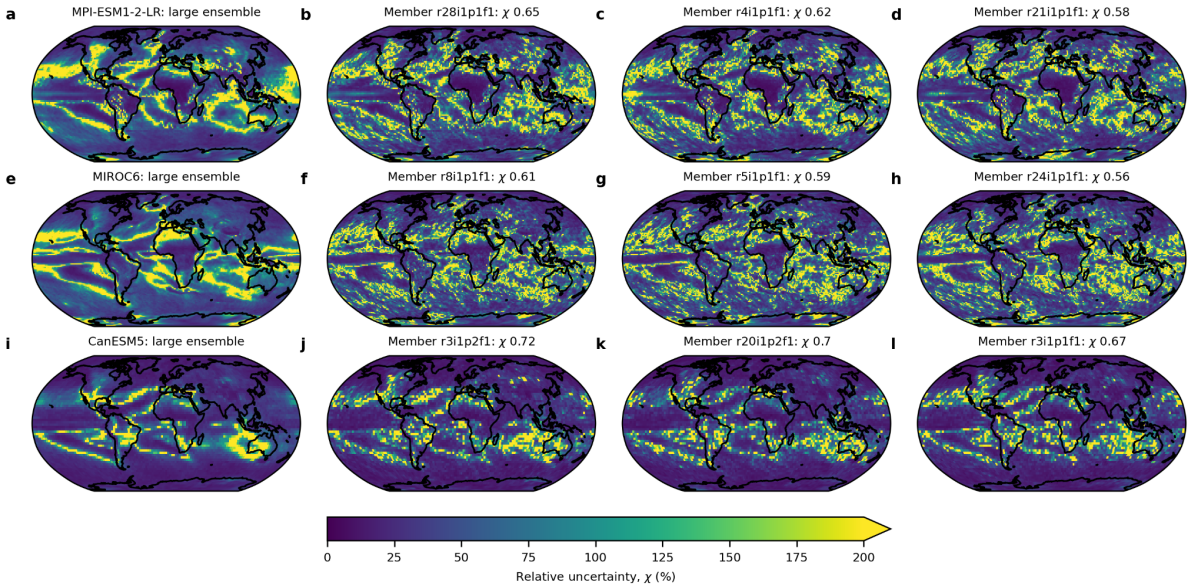



***Figure A14. Relative uncertainty in precipitation extreme intensity attribution due to internal variability using an extended time-series.*** As Figure A10 but using an extended time series of precipitation extreme intensity (*P5dx*) to from 1940-2100, using forcing from SSP5-8.5 from 2015-2100.



File generated with AMS Word template 2.0

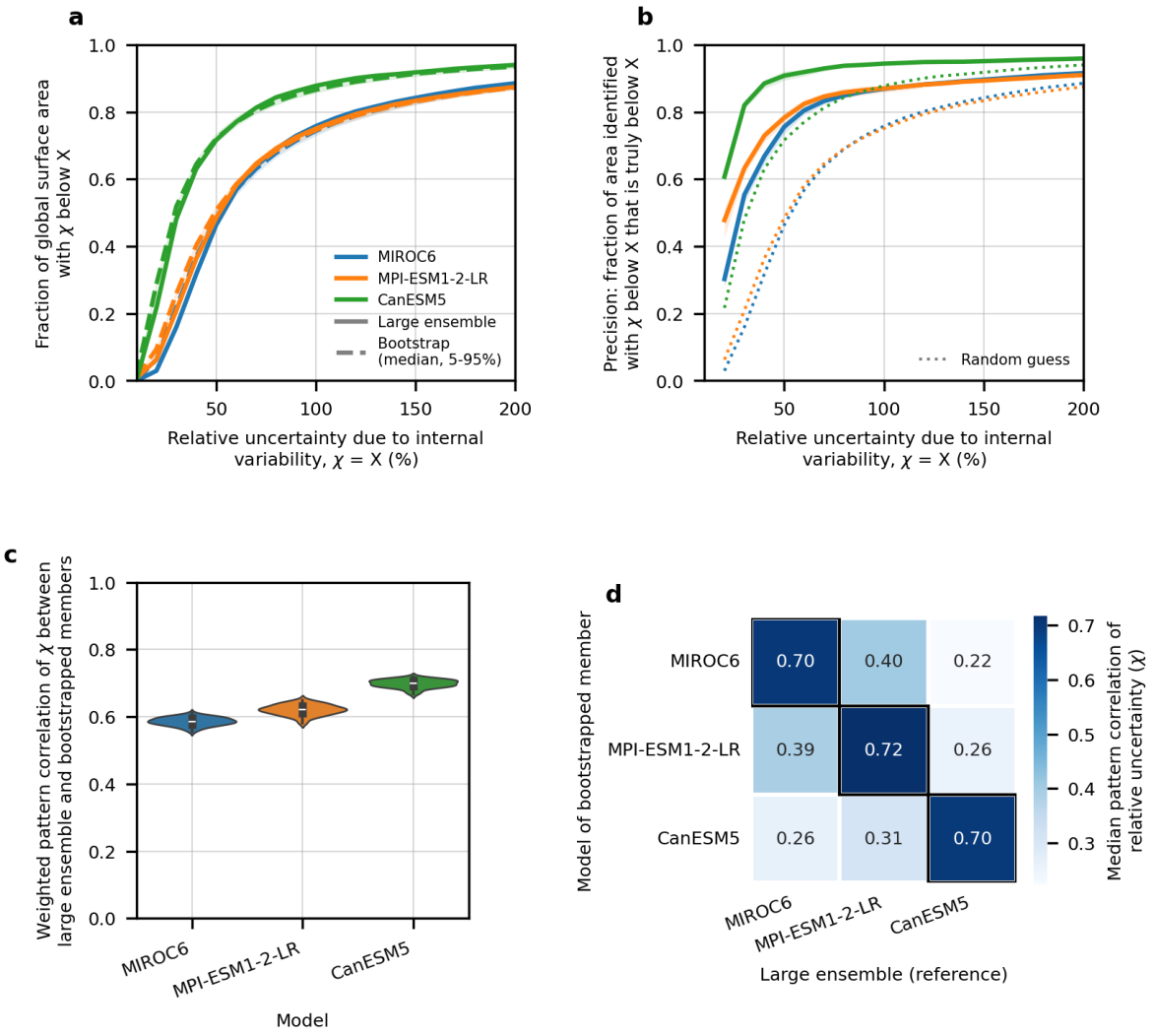



***Figure A15. Uncertainty in precipitation extreme intensity attribution with an extended time-series.*** As Figure A11 of the but using an extended time series of precipitation extreme intensity ( *P5dx*) to from 1940-2100, using forcing from SSP5-8.5 from 2015-2100.



File generated with AMS Word template 2.0

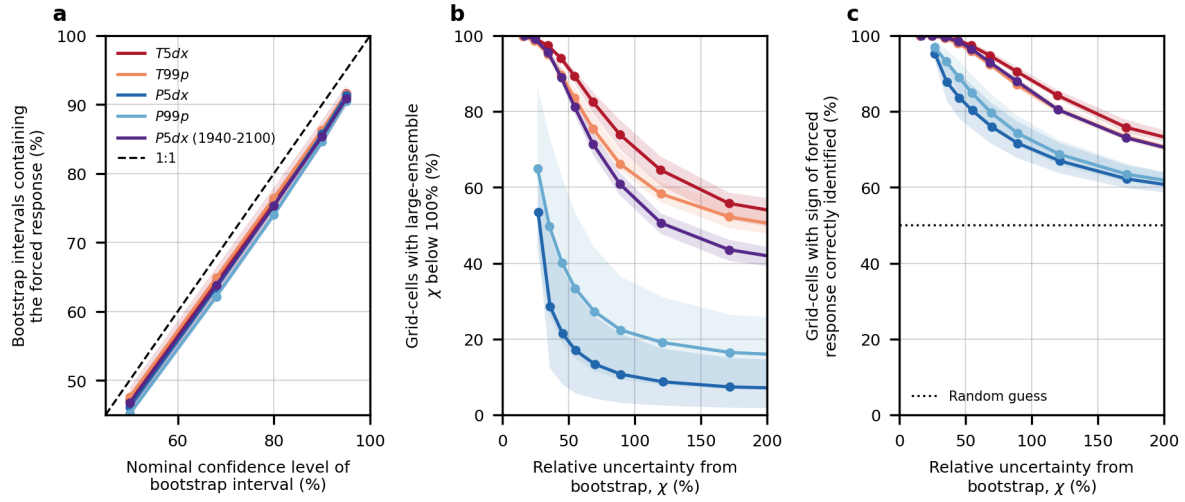



***Figure A16. Accuracy of block-bootstrap uncertainty estimates from individual ensemble members, taking the large ensemble as ground truth.*** *(a) The fraction of bootstrap confidence intervals of the linear-regression slope between global temperatures and local extremes which contain the large-ensemble mean slope, as a function of the nominal confidence level of the intervals (percentile intervals from 100 bootstrap samples, block width 5 years). The dashed line shows the 1:1 line of perfect calibration. (b) The fraction of grid-cells with a large-ensemble relative uncertainty below 100%, as a function of the relative uncertainty estimated by the bootstrap. (c) The fraction of grid-cells in which the sign of the bootstrapped slope matches that of the large-ensemble mean slope, as a function of the relative uncertainty estimated by the bootstrap. The dotted line shows the expectation from a random guess. All fractions are area-weighted and pooled across grid-cells and ensemble members. Lines show the mean across the three climate models and shading the range across models. In (b) and (c), grid-cells are binned by bootstrapped relative uncertainty and plotted at the area-weighted median of each bin, showing only bins which cover at least 0.5% of the global surface area in at least two models. Results are shown for the frequency (T99p, P99p) and intensity (T5dx, P5dx) of temperature and precipitation extremes over the historical period, and for P5dx over 1940–2100 using forcing from SSP5-8.5 from 2015.*



File generated with AMS Word template 2.0

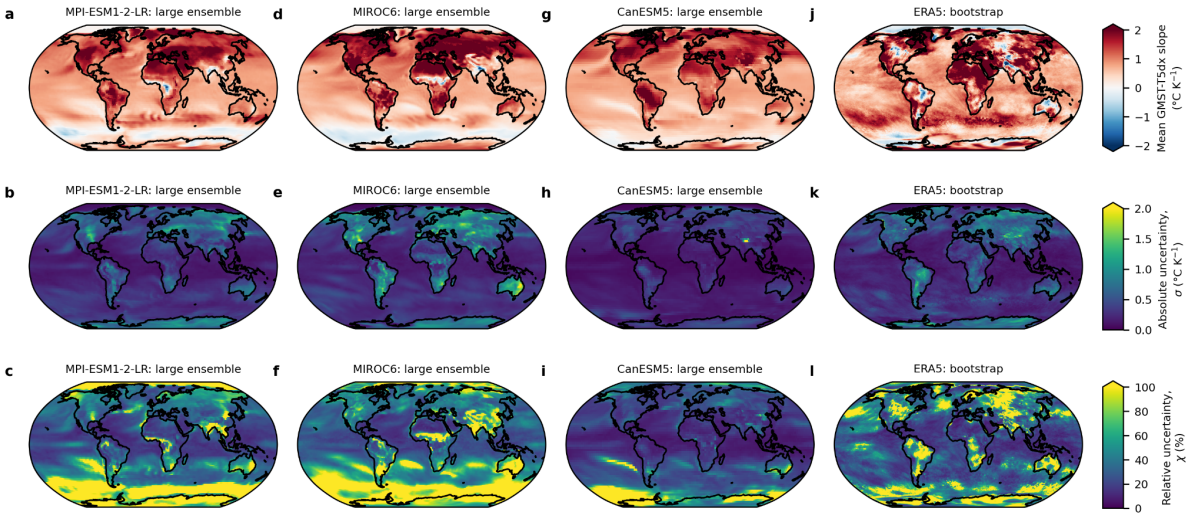



***Figure A17. Mean, absolute uncertainty and relative uncertainty of linear-regression slopes of heat extreme intensity on GMST.*** *The upper row shows the mean linear-regression slope between GMST and heat extreme intensity (T5dx), the middle row shows the standard deviation and the lower row the relative uncertainty of these slopes. Results are shown for the MPI-ESM1-2-LR (a-c), the MIROC6 (d-f) and CanESM5 large ensembles (g-i), as well as for the ERA5 reanalysis on the basis of the block-bootstrap procedure.*



File generated with AMS Word template 2.0

## APPENDIX B

### Relative uncertainty estimated from a single realisation

The relative uncertainty estimated by bootstrapping a single realisation (equation 4) can be written as:

$$\chi_{BS} = \frac{100\sigma_{BS}}{|\hat{\beta}_{BS}|} \approx \frac{100}{|\hat{t}|}, \text{ with } \hat{t} = \frac{\hat{\beta}}{\sigma_{BS}}, \quad \text{(B1)}$$

where $\hat{\beta}$ is the linear-regression slope estimated from the realisation (closely approximated by the bootstrap mean, $\hat{\beta}_{BS}$), such that $\hat{t}$ is the t-statistic of the slope. Equivalently, the large-ensemble relative uncertainty (equation 3) is the inverse of the true signal-to-noise ratio of the forced response:

$$\chi_{LE} = \frac{100}{|s|}, \text{ with } s = \frac{\mu}{\sigma}. \quad \text{(B2)}$$

The slope estimated from a single realisation can be considered as the ensemble mean plus a contribution from internal variability, $\hat{\beta} = \mu + \epsilon$ where $\epsilon$ has standard deviation $\sigma$. Provided the bootstrap captures this absolute uncertainty ($\sigma_{BS} \approx \sigma$, as shown in Figure 6), it follows that:

$$\hat{t} \approx s + z, \text{ with } z \sim N(0, 1). \quad \text{(B3)}$$

Where the signal-to-noise ratio is strong ($|s| \gg 1$), $|\hat{t}| \approx |s|$ and the bootstrap recovers the true relative uncertainty ($\chi_{BS} \approx \chi_{LE}$). Where the signal-to-noise ratio is weak ($s \approx 0$), $|\hat{t}| \approx |z|$ follows a half-normal distribution with median 0.674. The median bootstrapped relative uncertainty therefore saturates at:

$$\chi_{BS} \to \frac{100}{0.674} \approx 148\%, \quad \text{(B4)}$$



File generated with AMS Word template 2.0

847 regardless of how large the true relative uncertainty is. Bootstrapped relative uncertainties
848 well above ~150% are therefore not expected, and true relative uncertainties beyond 100%
849 are increasingly underestimated, as seen in Figure 5d.



File generated with AMS Word template 2.0

# REFERENCES


Allen, M., and Coauthors, 2019: Technical Summary: Global warming of 1.5 C. An IPCC Special Report on the impacts of global warming of 1.5 C above pre-industrial levels and related global greenhouse gas emission pathways, in the context of strengthening the global response to the threat of climate change, sustainable development, and efforts to eradicate poverty.

Arias, P., and Coauthors, 2021: Climate Change 2021: The Physical Science Basis. Contribution of Working Group14 I to the Sixth Assessment Report of the Intergovernmental Panel on Climate Change; Technical Summary.

Bartlett, M. S., 1946: On the theoretical specification and sampling properties of autocorrelated time-series. *Suppl. J. R. Stat. Soc.*, **8**, 27–41.

Beck, T. M., D. L. Schumacher, H. Achebak, A. M. Vicedo–Cabrera, S. I. Seneviratne, and J. Ballester, 2024: Mortality burden attributed to anthropogenic warming during Europe's 2022 record-breaking summer. *NPJ Clim. Atmospheric Sci.*, **7**, 245.

Bevacqua, E., C.-F. Schleussner, and J. Zscheischler, 2025: A year above 1.5 C signals that Earth is most probably within the 20-year period that will reach the Paris Agreement limit. *Nat. Clim. Change*, **15**, 262–265.

Callahan, C. W., and J. S. Mankin, 2022: Globally unequal effect of extreme heat on economic growth. *Sci. Adv.*, **8**, eadd3726.

Clarke, B., F. Otto, R. Stuart-Smith, and L. Harrington, 2022: Extreme weather impacts of climate change: an attribution perspective. *Environ. Res. Clim.*, **1**, 012001.

Davenport, F. V., M. Burke, and N. S. Diffenbaugh, 2021: Contribution of historical precipitation change to US flood damages. *Proc. Natl. Acad. Sci.*, **118**, e2017524118.

Deser, C., A. Phillips, V. Bourdette, and H. Teng, 2012: Uncertainty in climate change projections: the role of internal variability. *Clim. Dyn.*, **38**, 527–546.

Dimitrova, A., A. Dimitrova, M. Mengel, A. Gasparrini, H. Lotze-Campen, and S. Gabrysch, 2024: Temperature-related neonatal deaths attributable to climate change in 29 low-and middle-income countries. *Nat. Commun.*, **15**, 5504.

Donat, M. G., C. Delgado-Torres, P. De Luca, R. Mahmood, P. Ortega, and F. J. Doblas-Reyes, 2023: How credibly do CMIP6 simulations capture historical mean and extreme precipitation changes? *Geophys. Res. Lett.*, **50**, e2022GL102466.

Erazo, D., and Coauthors, 2024: Contribution of climate change to the spatial expansion of West Nile virus in Europe. *Nat. Commun.*, **15**, 1196.

Eyring, V., S. Bony, G. A. Meehl, C. A. Senior, B. Stevens, R. J. Stouffer, and K. E. Taylor, 2016: Overview of the Coupled Model Intercomparison Project Phase 6 (CMIP6) experimental design and organization. *Geosci. Model Dev.*, **9**, 1937–1958.





File generated with AMS Word template 2.0

Fischer, E. M., U. Beyerle, and R. Knutti, 2013: Robust spatially aggregated projections of climate extremes. *Nat. Clim. Change*, **3**, 1033–1038.

Gillett, N. P., and Coauthors, 2016: The detection and attribution model intercomparison project (DAMIP v1. 0) contribution to CMIP6. *Geosci. Model Dev.*, **9**, 3685–3697.

Hawkins, E., and R. Sutton, 2009: The potential to narrow uncertainty in regional climate predictions. *Bull. Am. Meteorol. Soc.*, **90**, 1095–1108.

Hegerl, G. C., Han. voN SToRcH, K. Hasselmann, B. D. Santer, U. Cubasch, and P. D. Jones, 1996: Detecting greenhouse-gas-induced climate change with an optimal fingerprint method. *J. Clim.*, **9**, 2281–2306.

Hegerl, G. C., and Coauthors, 2007: Understanding and attributing climate change. *Contrib. Work. Group Fourth Assess. Rep. Intergov. Panel Clim. Change IPCC Solomon Qin M Manning Z Chen M Marquis KB Averyt M Tignor HL Mill. Eds Camb. Univ. Press Camb. U. K. N. Y. NY USA 996 Pp*.

Hersbach, H., and Coauthors, 2020: The ERA5 global reanalysis. *Q. J. R. Meteorol. Soc.*, **146**, 1999–2049.

King, A. D., M. R. Grose, J. Kimutai, I. Pinto, and L. J. Harrington, 2023: Event attribution is not ready for a major role in loss and damage. *Nat. Clim. Change*, **13**, 415–417.

Kotz, M., A. Levermann, and L. Wenz, 2022: The effect of rainfall changes on economic production. *Nature*, **601**, 223–227.

Kotz. M., T. Amano, and J. E. Watson, 2025: Large reductions in tropical bird abundance attributable to heat extreme intensification. *Nat. Ecol. Evol.*, 1–13.

Lee, H., and Coauthors, 2023: IPCC, 2023: Climate change 2023: Synthesis report, summary for policymakers. Contribution of working groups i, II and III to the sixth assessment report of the intergovernmental panel on climate change [core writing team, h. Lee and j. Romero (eds.)]. IPCC, geneva, Switzerland.

Lehner, F., C. Deser, N. Maher, J. Marotzke, E. M. Fischer, L. Brunner, R. Knutti, and E. Hawkins, 2020: Partitioning climate projection uncertainty with multiple large ensembles and CMIP5/6. *Earth Syst. Dyn.*, **11**, 491–508.

Marcos, M., A. Amores, M. Agulles, J. Robson, and X. Feng, 2025: Global warming drives a threefold increase in persistence and 1° C rise in intensity of marine heatwaves. *Proc. Natl. Acad. Sci.*, **122**, e2413505122.

McKinnon, K. A., and C. Deser, 2018: Internal variability and regional climate trends in an observational large ensemble. *J. Clim.*, **31**, 6783–6802.

McKinnon, K. A., A. Poppick, E. Dunn-Sigouin, and C. Deser, 2017: An “observational large ensemble” to compare observed and modeled temperature trend uncertainty due to internal variability. *J. Clim.*, **30**, 7585–7598.



File generated with AMS Word template 2.0

Mengel, M., S. Treu, S. Lange, and K. Frieler, 2021: ATTRICI v1. 1–counterfactual climate for impact attribution. *Geosci. Model Dev.*, **14**, 5269–5284.

Murali, G., T. Iwamura, S. Meiri, and U. Roll, 2023: Future temperature extremes threaten land vertebrates. *Nature*, **615**, 461–467.

Noy, I., M. Wehner, D. Stone, S. Rosier, D. Frame, K. A. Lawal, and R. Newman, 2023: Event attribution is ready to inform loss and damage negotiations. *Nat. Clim. Change*, **13**, 1279–1281.

Paik, S., S.-K. Min, X. Zhang, M. G. Donat, A. D. King, and Q. Sun, 2020: Determining the anthropogenic greenhouse gas contribution to the observed intensification of extreme precipitation. *Geophys. Res. Lett.*, **47**, e2019GL086875.

Pfahl, S., P. A. O'Gorman, and E. M. Fischer, 2017: Understanding the regional pattern of projected future changes in extreme precipitation. *Nat. Clim. Change*, **7**, 423–427.

Pfleiderer, P., C.-F. Schleussner, and J. Sillmann, 2024: Limited reversal of regional climate signals in overshoot scenarios. *Environ. Res. Clim.*, **3**, 015005.

Riahi, K., and Coauthors, 2017: The shared socioeconomic pathways and their energy, land use, and greenhouse gas emissions implications: an overview. *Glob. Environ. Change*, **42**, 153–168.

Roldán-Gómez, P. J., P. De Luca, R. Bernardello, and M. G. Donat, 2025: Regional irreversibility of mean and extreme surface air temperature and precipitation in CMIP6 overshoot scenarios associated with interhemispheric temperature asymmetries. *Earth Syst. Dyn.*, **16**, 1–27.

Seneviratne, S. I., M. G. Donat, A. J. Pitman, R. Knutti, and R. L. Wilby, 2016: Allowable CO2 emissions based on regional and impact-related climate targets. *Nature*, **529**, 477–483.

Swart, N. C., and Coauthors, 2019: The Canadian earth system model version 5 (CanESM5. 0.3). *Geosci. Model Dev.*, **12**, 4823–4873.

Trok, J. T., E. A. Barnes, F. V. Davenport, and N. S. Diffenbaugh, 2024: Machine learning–based extreme event attribution. *Sci. Adv.*, **10**, eadl3242.

Van Oldenborgh, G. J., and Coauthors, 2021: Pathways and pitfalls in extreme event attribution. *Clim. Change*, **166**, 13.

Wang, K., X. Liu, P. Cui, Y. Zhang, J. Xie, C. Liu, and S. N. Gosling, 2025: China's nationwide streamflow decline driven by landscape changes and human interventions. *Sci. Adv.*, **11**, eadu8032.

Wills, R. C., Y. Dong, C. Proistosecu, K. C. Armour, and D. S. Battisti, 2022: Systematic climate model biases in the large-scale patterns of recent sea-surface temperature and sea-level pressure change. *Geophys. Res. Lett.*, **49**, e2022GL100011.



File generated with AMS Word template 2.0

Wills, R. C., and Coauthors, 2025: Forced Component Estimation Statistical Method Intercomparison Project (ForceSMIP). *Authorea Prepr.*

Zhang, W., K. Furtado, P. Wu, T. Zhou, R. Chadwick, C. Marzin, J. Rostron, and D. Sexton, 2021: Increasing precipitation variability on daily-to-multiyear time scales in a warmer world. *Sci. Adv.*, **7**, eabf8021.